

Approximating f -Divergences with Rank Statistics

Viktor Stein*[†]

José Manuel de Frutos[†]

February 2, 2026

Abstract

We introduce a rank-statistic approximation of f -divergences that avoids explicit density-ratio estimation by working directly with the distribution of ranks. For a resolution parameter K , we map the mismatch between two univariate distributions μ and ν to a rank histogram on $\{0, \dots, K\}$ and measure its deviation from uniformity via a discrete f -divergence, yielding a rank-statistic divergence estimator. We prove that the resulting estimator of the divergence is monotone in K , is always a lower bound of the true f -divergence, and we establish quantitative convergence rates for $K \rightarrow \infty$ under mild regularity of the quantile-domain density ratio. To handle high-dimensional data, we define the sliced rank-statistic f -divergence by averaging the univariate construction over random projections, and we provide convergence results for the sliced limit as well. We also derive finite-sample deviation bounds along with asymptotic normality results for the estimator. Finally, we empirically validate the approach by benchmarking against neural baselines and illustrating its use as a learning objective in generative modelling experiments.

1 Introduction

Quantifying discrepancy between probability distributions is fundamental in statistics and machine learning. A prominent and widely used class of such measures is given by f -divergences, defined in (1), which include the Kullback–Leibler divergence, total variation, Hellinger, and χ^2 -type divergences [1, 10]. They arise throughout the field, from hypothesis testing and model comparison to variational objectives for implicit generative modelling [19, 40]. However, reliably estimating f -divergences from samples is challenging: most formulations depend on the density ratio $\frac{d\mu}{d\nu}$, so approaches that first estimate the densities (or their ratio) and then substitute can suffer from severe statistical error in moderate-to-high dimensions [35, 45].

A common workaround is to estimate f -divergences via *variational* formulations, which recast divergence estimation as (regularized) risk minimization and, in many cases, as a classification-style objective [38, 40, 46]. Related principles include noise-contrastive estimation for unnormalized models [21] and neural variational estimators based on Donsker–Varadhan-type objectives, popularized in the mutual-information literature [5]. In practice, however, these approaches may require delicate function-class choices and optimization heuristics, and can inherit the instabilities associated with adversarial/variational training [3, 20].

*Institute of Mathematics, Technische Universität Berlin, Straße des 17. Juni 136, 10623 Berlin, Germany, stein@math.tu-berlin.de, <https://tu.berlin/imageanalysis>

[†]Department of Signal Theory and Communications, Universidad Carlos III, Madrid, Spain. jofrutos@ing.uc3m.es

A different line of work mitigates high-dimensional difficulties by comparing *one-dimensional projections* of distributions and aggregating the resulting discrepancies. The sliced Wasserstein distance and its extensions are prominent examples in generative modelling, offering favourable computational scaling by reducing multivariate comparisons to repeated 1D problems [24, 54]. More generally, sliced probability divergences have been studied from statistical and topological viewpoints [37]. These ideas suggest that if one can build a robust and scalable 1D divergence estimator, then slicing can lift it to higher dimensions.

In this paper, we develop a *rank-statistic* approximation of f -divergences. The construction starts from a fixed reference measure ν and uses the (univariate) probability integral transform (PIT): if $X \sim \nu$, then $F_\nu(X)$ is uniform on $[0, 1]$ [23, 44, 49]. Uniformity diagnostics based on PIT/rank histograms are standard tools in forecast calibration and reliability assessment [18, 22]. We turn this principle into a general divergence construction: we discretize the PIT into a *rank histogram* with K bins and measure its deviation from uniformity via an entropic function f . For a related construction to approximate the CDF of a probability density, see [28]. The resulting rank-statistic divergence is bounded, depends only on *order information*, and admits simple estimators built from sorting and counting operations. We then extend it to \mathbb{R}^d by averaging over random 1D projections, yielding *sliced rank-statistic f -divergences* in the spirit of [4, 24, 37].

1.1 Contributions

The main results of this paper are the following:

- We propose a rank-histogram approximation $D_{f,\nu}^{(K)}(\mu)$ of the f -divergence, parametrized by a resolution K , generalizing the works [11–13], enabling us to compare different choices of entropy function f . In particular, we can choose differentiable functions f , which better interact with automatic differentiation schedules used for learning tasks. It is an optimization-free estimator of the (sliced) f -divergence.
- We establish basic regularity properties, and show that $D_{f,\nu}^{(K)}(\mu)$ is nondecreasing in K and dominated by $D_{f,\nu}(\mu)$. Under mild assumptions on the density ratio, we prove consistency as $K \rightarrow \infty$ and provide quantitative approximation rates. We also derive finite-sample deviation bounds for the univariate estimator and prove asymptotic normality.
- We define sliced rank-statistic f -divergences in \mathbb{R}^d by averaging the univariate construction over random 1D projections, thereby inheriting its key univariate properties.
- We benchmark against classical and neural baselines on synthetic tasks, showing that rank-statistic f -divergences provide stable approximations of the target f -divergence that perform well in high dimensions and with few samples. Our generative transport algorithm shows that the rank-statistic f -divergence can serve as effective learning objectives for implicit models, showcased on two-dimensional toy models and on the CelebA and MNIST dataset.

Notation By \mathbb{N} we denote the non-negative integers. For $K \in \mathbb{N}$ we set $[K] := \{0, \dots, K\}$. The uniform distribution on $[K]$ is denoted by U_K . The quantile function of a univariate probability measure $\mu \in \mathcal{P}(\mathbb{R})$ is denoted by Q_μ and its CDF by R_μ . The expectation of a function f under $\mu \in \mathcal{P}(\mathbb{R}^d)$ is denoted by $\mathbb{E}_\mu[f] := \int_{\mathbb{R}^d} f(x) d\mu(x)$. The pushforward is denoted by $\#$. We denote by \mathcal{C}^k the k -times continuously differentiable functions and by $\mathcal{C}^{0,\alpha}$ the α -Hölder continuous functions.

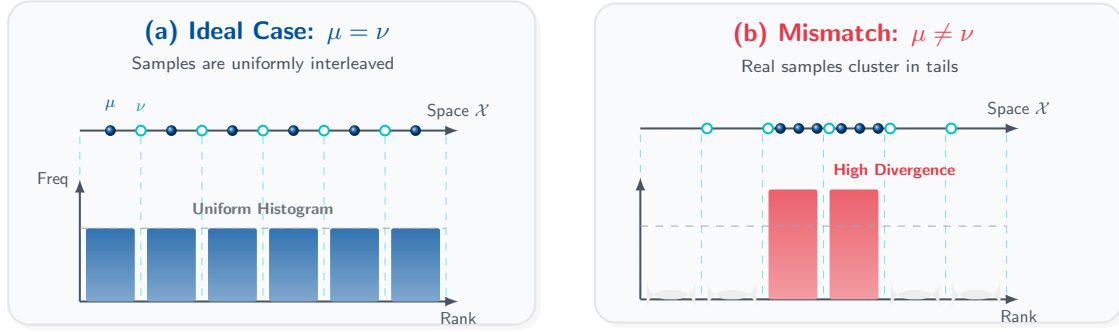


Figure 1: Conceptual illustration of the rank-statistic f -divergence. (a) When $\mu = \nu$, samples are uniformly interleaved, resulting in a uniform rank histogram. (b) With a mismatch, samples from μ cluster in specific rank bins, creating a non-uniform histogram that indicates divergence.

2 Rank-based approximation of one-dimensional f -divergences

We begin with the one-dimensional setting and introduce a rank-based approximation of f -divergences. The construction relies on the integral probability transform and a discrete rank histogram which encodes the mismatch between a distribution μ and a target ν .

In this section, let $\mu, \nu \in \mathcal{P}(\mathbb{R})$ be univariate probability measures. In the following, let $f: [0, \infty) \rightarrow \mathbb{R} \cup \{+\infty\}$ always be a convex, lower semicontinuous function with $f(1) = 0$ and $\lim_{t \rightarrow \infty} \frac{1}{t} f(t) > 0$. We then say that f is an *entropy function*. Note that due to convexity, f is Lipschitz on any compact set $K \subset (0, \infty)$.

The (continuous) f -divergence of μ with respect to ν is

$$D_{f,\nu}(\mu) := \begin{cases} \int f\left(\frac{d\mu}{d\nu}(x)\right) d\nu(x), & \text{if } \mu \ll \nu, \\ +\infty, & \text{otherwise.} \end{cases} \quad (1)$$

Directly working with $\frac{d\mu}{d\nu}$ is often inconvenient. Instead, we approximate $D_{f,\nu}(\mu)$ using a simple rank statistic of μ relative to ν .

Definition 2.1. Fix $K \in \mathbb{N}$. Let $Y \sim \mu$ and $\tilde{Y}_1, \dots, \tilde{Y}_K \stackrel{\text{i.i.d.}}{\sim} \nu$, independent of Y . The *rank statistic of order K* of μ with respect to ν is

$$A_{\mu|\nu}^{(K)} := \#\{j \in [K] : \tilde{Y}_j \leq Y\} \in [K]. \quad (2)$$

We denote by $Q_{\mu|\nu}^{(K)}$ the probability mass function (pmf) of $A_{\mu|\nu}^{(K)}$ on $[K]$.

When $\mu \ll \nu$, then $\mu = \nu$ if and only if the rank statistic is uniform, i.e., $Q_{\nu|\nu}^{(K)}(n) \equiv 1/(K+1)$, for all $K \in \mathbb{N}$, see Lemma B.1.

The pmf $Q_{\mu|\nu}^{(K)}$ can be seen as a discrete ‘‘rank histogram’’ of μ with respect to ν . It records how often a draw from μ falls below $0, 1, \dots, K$ i.i.d. draws from ν . Departures of this histogram from the uniform law signal discrepancies between μ and ν .

To quantify the discrepancy of the rank histogram from uniformity, we use a discrete f -divergence, see also Remark B.2.

Definition 2.2. Let U_K denote the uniform distribution on $[K]$. The *rank-statistic f -divergence of order K* of μ to ν is

$$D_{f,\nu}^{(K)}(\mu) := D_f(Q_{\mu|\nu}^{(K)} \| U_K) = \frac{1}{K+1} \sum_{n=0}^K f((K+1)Q_{\mu|\nu}^{(K)}(n)),$$

where $D_f(\cdot\|\cdot)$ is the discrete f -divergence on the finite alphabet $[K]$.

Example 2.1. For the entropy function $f_{\text{TV}} := |\cdot - 1|$ of the total variation divergence, Definition 2.2 recovers the ISL discrepancy d_K from [11], up to a prefactor: $D_{f_{\text{TV}},\nu}^{(K)}(\mu) = (K+1)d_K(\mu, \nu)$,

Empirical estimation of rank-statistic f -divergences In applications we only observe samples, so we estimate the rank pmf $Q_{\mu|\nu}^{(K)}$ by a simple count-based procedure. For each $X_i \sim \hat{\mu}_N$, draw $\tilde{Y}_1, \dots, \tilde{Y}_K \sim \hat{\nu}_M$ (e.g. by sampling with replacement from $\{Y_j\}_{j=1}^M$), compute the rank count

$$a_i := \#\{j \in [K] : \tilde{Y}_j \leq X_i\} \in [K],$$

and increment bin a_i of a histogram $Q[0:K]$. Normalizing by N yields a pmf estimate Q , which we plug into (3) to obtain the empirical divergence.

Now, we collect basic properties of the rank-statistic f -divergence, in particular that $D_{f,\nu}^{(K)}$ is monotone in the rank resolution K and that, similarly to $D_{f,\nu}$, the approximation $D_{f,\nu}^{(K)}$ inherits regularity properties from f . The second inequality below generalizes [11, Thm. 2] [13, Thm. 2.2].

Theorem 2.3. Let $\mu, \nu \in \mathcal{P}(\mathbb{R})$ and $K \in \mathbb{N}$. The map $D_{f,\nu}^{(K)}$ is convex and if Q_ν is continuous, it is also weakly lower semicontinuous. Furthermore,

$$D_{f,\nu}^{(K)}(\mu) \leq D_{f,\nu}^{(K+1)}(\mu) \leq D_{f,\nu}(\mu). \quad (3)$$

Proof. See Section B.2. □

Remark 2.4 (Markov kernel interpretation of $D_f^{(K)}$). One can also prove (3) by noticing that the Markov kernel $\kappa: [K] \times \mathbb{R} \rightarrow [0, 1]$, $(n \mid y) \mapsto (b_{n,K} \circ R_\nu)(y)$ fulfills $D_{f,\kappa \circ \nu}(\kappa \circ \mu) = D_{f,\nu}^{(K)}(\mu)$ and then use the data processing inequality for f -divergences (Lemma A.2). We also have $D_{f,T_\# \nu}^{(K)}(T_\# \mu) = D_{f,\nu}^{(K)}(\mu)$ for strictly increasing functions $T: \mathbb{R} \rightarrow \mathbb{R}$.

2.1 Approximation properties

We are interested in the behaviour of the increasing sequence $\{D_{f,\nu}^{(K)}(\mu)\}_{K \in \mathbb{N}}$ as the resolution parameter K grows. Intuitively, increasing K refines the rank histogram, so one expects the discrete quantity $D_{f,\nu}^{(K)}(\mu)$ to approach the continuous f -divergence $D_{f,\nu}(\mu)$. This is indeed the case under a mild regularity assumption on the rank density ratio r , whose regularity determines the convergence rates precisely in the way that it determines the convergence rate of the Bernstein approximation $\|B_K[r] - r\|_\infty$, see Section A.

Theorem 2.5 (Convergence of the truncated divergence). *If $\mu \ll \nu$ and $r := r_{\mu|\nu} := \frac{d\mu}{d\nu} \circ Q_\nu \in \mathcal{C}([0, 1])$ and f is L_f -Lipschitz on $\text{ran}(r)$, then for $K \rightarrow \infty$,*

$$D_{f,\nu}(\mu) - D_{f,\nu}^{(K)}(\mu) \begin{cases} \rightarrow 0, & \text{if } r \in \mathcal{C}([0, 1]), \\ \in O(K^{-\frac{\alpha}{2}}), & \text{if } r \in C^{0,\alpha}([0, 1]), \\ \in O(K^{-1}), & \text{if } r \in \mathcal{C}^2([0, 1]), \text{ or} \\ & \text{if } r \text{ is Lipschitz and} \\ & f \in \mathcal{C}^2([0, \infty)). \end{cases}$$

Proof. Consider the piecewise-constant function

$$r_K(u) := c_K(n) := (K+1)Q_{\mu|\nu}^{(K)}(n)$$

for $u \in \left[\frac{n}{K+1}, \frac{n+1}{K+1}\right)$, $n \in [K]$. Then,

$$D_{f,\nu}^{(K)}(\mu) = \frac{1}{K+1} \sum_{n=0}^K f((K+1)Q_{\mu|\nu}^{(K)}(n)) = \int_0^1 f(r_K(u)) \, du.$$

In Section B.3, we prove that r_K converges uniformly to r and prove the rates. The result then follows from

$$D_{f,\nu}(\mu) - D_{f,\nu}^{(K)}(\mu) \leq \int_0^1 |f(r_K(u)) - f(r(u))| \, du \leq L_f \|r_K - r\|_\infty. \quad \square$$

We examine the applicability of Theorem 2.5 to standard f -divergences.

Example 2.2 (Applicability of Convergence Rates). The entropy function f_{TV} is the only globally Lipschitz one (up to scalar prefactors).

- If $0 \notin \text{ran}(r)$, then the $O(K^{-\frac{\alpha}{2}})$ rate is achieved for most divergences (including KL, Jensen–Shannon, squared Hellinger, and Jeffreys) since they are Lipschitz away from zero.
- the fast rate $O(K^{-1})$ is obtained if $f \in \mathcal{C}^2([0, \infty))$ which excludes KL and Hellinger and $|\cdot - 1|^\alpha$, for $\alpha > 1$, but holds for the χ^2 -divergence (with $f_{\chi^2}(t) = \frac{1}{2}(t-1)^2$) and other polynomial (“Tsallis”)–entropy functions, and the triangular discrimination generator $f(t) = \frac{(t-1)^2}{t+1}$ [30].

For a long list of choices of f , see [52, Tab. 1].

2.2 Finite-sample bounds

We now study the finite-sample properties of the rank-based f -divergence estimator. Given sample sizes $N, M \in \mathbb{N}$, let $(X_j)_{j=1}^N \stackrel{\text{i.i.d.}}{\sim} \mu$ and $(Y_k)_{k=1}^M \stackrel{\text{i.i.d.}}{\sim} \nu$. We define the corresponding empirical measures as

$$\mu_N := \frac{1}{N} \sum_{i=1}^N \delta_{X_i}, \quad \nu_M := \frac{1}{M} \sum_{j=1}^M \delta_{Y_j}. \quad (4)$$

Theorem 2.6 (Univariate finite sample complexity). *Let $\mu, \nu \in \mathcal{P}(\mathbb{R})$ and $\hat{\mu}_N$ and $\hat{\nu}_M$ be their corresponding empirical measures with sample sizes N and M . For a fixed rank resolution K , if f is L_f -Lipschitz on $[0, K+1]$, then the expected estimation error satisfies*

$$\mathbb{E} \left[\left| D_{f, \hat{\nu}_M}^{(K)}(\hat{\mu}_N) - D_{f, \nu}^{(K)}(\mu) \right| \right] \leq L_f(K+1) \sqrt{2\pi} \left(\frac{1}{\sqrt{N}} + \frac{1}{\sqrt{M}} \right).$$

Proof. See Section B.6. □

Proposition 2.7 (Concentration bound). *Let $K \in \mathbb{N}$ be fixed, and let $\hat{\mu}_N, \hat{\nu}_M$ be the empirical measures based on N and M i.i.d. samples from $\mu, \nu \in \mathcal{P}(\mathbb{R})$, respectively. If f is L_f -Lipschitz on $[0, K+1]$, then for any $\delta > 0$, with probability at least $1 - \delta$, we have*

$$\left| D_{f, \hat{\nu}_M}^{(K)}(\hat{\mu}_N) - \mathbb{E}[D_{f, \hat{\nu}_M}^{(K)}(\hat{\mu}_N)] \right| \leq L_f(K+1) \sqrt{2 \log(2/\delta) \left(\frac{1}{N} + \frac{1}{M} \right)}.$$

Proof. See Section B.7. □

3 Sliced rank-based f -divergences in higher dimensions

We now extend the rank-statistic f -divergence from Definition 2.2 to the d -dimensional setting via *slicing*. The idea is to reduce the high-dimensional discrepancy between μ and ν to a collection of one-dimensional discrepancies along suitably chosen projections, in the spirit of sliced Wasserstein distances and related constructions. Throughout this section we work with one-dimensional projections along unit directions on the sphere.

For $s \in \mathbb{S}^{d-1}$, let $\mu_s := s\#\mu$ be the one-dimensional pushforward of μ by $x \mapsto s^\top x$. For fixed $K \in \mathbb{N}$, Definition 2.2 yields a univariate rank-statistic f -divergence $D_f^{(K)}(\mu_s \mid \nu_s)$ describing the mismatch between μ_s and ν_s .

Definition 3.1 (Sliced rank-statistic f -divergence). *Let $\mu, \nu \in \mathcal{P}(\mathbb{R}^d)$ with $\mu \ll \nu$. Let σ denote the uniform probability measure on \mathbb{S}^{d-1} . The *sliced rank-statistic f -divergence* of order K and the *sliced f -divergence* are, resp.*

$$\begin{aligned} D_{f, \nu}^{(K)}(\mu) &:= \int_{\mathbb{S}^{d-1}} D_{f, \nu_s}^{(K)}(\mu_s) d\sigma(s), \\ \text{SD}_{f, \nu}(\mu) &:= \int_{\mathbb{S}^{d-1}} D_{f, \nu_s}(\mu_s) d\sigma(s). \end{aligned}$$

The next result states that the results from the previous section carry over to the sliced construction.

Theorem 3.2. *The map $D_{f, \nu}^{(K)}$ is convex. Let $\mu, \nu \in \mathcal{P}(\mathbb{R}^d)$ with $\mu \ll \nu$. Then,*

$$D_{f, \nu}^{(K)}(\mu) \leq \text{SD}_{f, \nu}(\mu) \leq D_{f, \nu}(\mu), \quad K \in \mathbb{N}. \quad (5)$$

If $r_{\mu_s \mid \nu_s} \in \mathcal{C}([0, 1])$ for almost all $s \in \mathbb{S}^{d-1}$, then

$$\lim_{K \rightarrow \infty} D_{f, \nu}^{(K)}(\mu) = \text{SD}_{f, \nu}(\mu),$$

Proof. See Section B.4. □

Now, we examine the variance of the estimator $D_{f,\nu}^{(K)}$ when estimating its input by samples.

Theorem 3.3 (Asymptotic normality, sliced one-sample case). *Fix $K \in \mathbb{N}$ and $\mu, \nu \in \mathcal{P}(\mathbb{R}^d)$ with $\mu \neq \nu$ and $D_{f,\nu}^{(K)}(\mu) > 0$, and form the empirical approximation $\hat{\mu}_N$ from (4). If $f \in \mathcal{C}^1([0, K+1])$, then there exists a constant $\tau_K^2 > 0$ such that, in distribution,*

$$\sqrt{N} \left(D_{f,\nu}^{(K)}(\hat{\mu}_N) - D_{f,\nu}^{(K)}(\mu) \right) \xrightarrow[N \rightarrow \infty]{d} \mathcal{N}(0, \tau_K^2).$$

Proof. See Section B.8. □

4 Experiments

We evaluate the proposed rank-statistic f -divergence estimator across synthetic and high-dimensional settings. Our experiments quantify estimation accuracy, sensitivity to the resolution parameter K , and the benefits of the sliced extension. We also demonstrate its practical behavior when used as a fully sample-based objective in downstream learning on the CelebA data set [31]. We defer many more experiments to Section C.

4.1 Neural vs. rank-statistic divergence estimation across dimensions

We benchmark the proposed rank-statistic f -divergence estimator on the same synthetic setup as the neural KL-divergence estimator of [51], using their training protocol for all sample sizes (optimizer, architecture scaling, and training schedule), taking μ and ν as (suitably truncated) standard Gaussian and uniform distributions, respectively (details are deferred to Section C.1).

In contrast to the neural baseline, our rank-statistic estimator involves no iterative optimization: once the samples are fixed, it is fully determined by the rank resolution K and the number of projections L .

Since both μ and ν factorize over coordinates (independent Gaussian components and a product-box truncation),

$$\text{KL}(\mu\|\nu) = \sum_{j=1}^d \text{KL}(\mu_j\|\nu_j).$$

Accordingly, an axis-corrected rank estimator is used: compute the 1D degree- K terms $D_{f_{\text{KL}},\nu_j}^{(K)}(\mu_j)$ and sum them up:

$$D_{\text{KL},\text{axis}}^{(K)}(\mu\|\nu) := \sum_{j=1}^d D_{f_{\text{KL}},\nu_j}^{(K)}(\mu_j).$$

This leverages the fact that the coordinate axes already capture the discrepancy, without averaging over random projections.

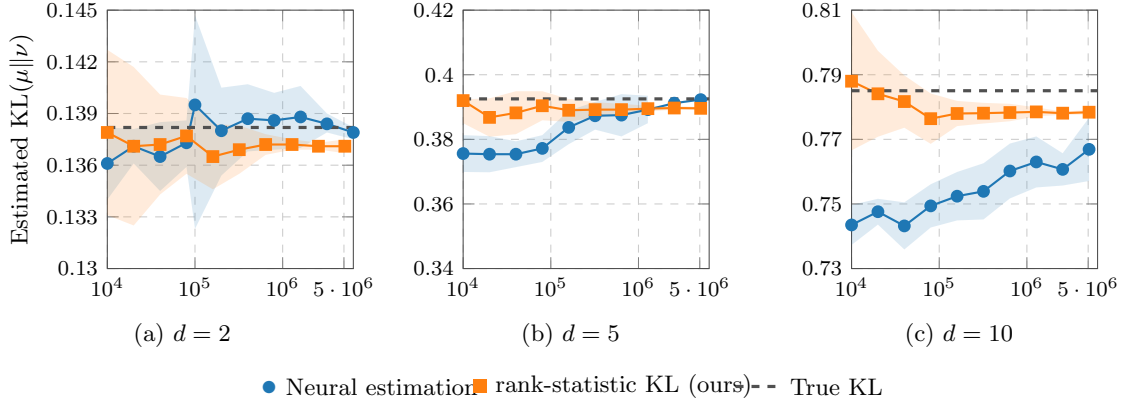


Figure 2: Convergence of Kullback–Leibler divergence estimates for increasing sample size n , averaged over 10 independent runs. Shaded bands denote the ± 1 standard deviation interval. Results are shown for $K = 64$ across all samples.

Evaluation and plots. For each dimension, Figure 2 reports the estimated $\text{KL}(\mu\|\nu)$ as a function of the sample size n , for both the neural baseline and the rank-statistic estimator. The ground-truth $\text{KL}(\mu\|\nu)$ (dashed horizontal line) is computed analytically (implementation details are deferred to Section C.1).

Across all $d \in \{2, 5, 10\}$, the rank-statistic estimator tracks the analytic reference closely and becomes increasingly stable as n grows, with the uncertainty band contracting rapidly; in particular, it is already accurate in the smaller- n regime (most noticeably for $d = 5$ and $d = 10$), where it provides a useful signal before the neural baseline has stabilized. The neural estimator exhibits larger variability and more noticeable deviations from the reference, especially in higher dimension, suggesting that neural f -divergence estimation requires a larger sample budget to become reliable in this setting. Overall, these results indicate that the rank-statistic approach is competitive on this benchmark, often offering smoother and more data-efficient estimates while avoiding iterative training.

4.2 Univariate empirical convergence and the influence of the resolution parameter K

This subsection benchmarks the one-dimensional rank-statistic estimator against standard f -divergences in settings where accurate reference values are available, and studies how the finite resolution parameter K controls the approximation gap. We focus on three widely used discrepancies, Kullback–Leibler (KL), Jensen–Shannon (JS) [29], and the squared Hellinger divergence, and consider four representative mismatch families: (i) Gaussian mean shifts: $\mathcal{N}(0, 1)$ vs. $\mathcal{N}(\Delta, 1)$ with $\Delta \in \{0, 0.5, 1, 2\}$ (JS and KL); (ii) Gaussian scale changes: $\mathcal{N}(0, 1)$ vs. $\mathcal{N}(0, \sigma)$ with $\sigma \in \{1, 1.2, 1.5, 2\}$ (KL and squared Hellinger); (iii) a symmetric Gaussian mixture: $\frac{1}{2}\mathcal{N}(-\Delta, 1) + \frac{1}{2}\mathcal{N}(+\Delta, 1)$ vs. $\mathcal{N}(0, 1)$ (JS); and (iv) a tail-mismatch case of Laplace(0, 1) vs. $\mathcal{N}(0, 1)$ (JS).

Reference values use closed forms when available (Gaussian–Gaussian KL and squared Hellinger), and otherwise a high-accuracy one-dimensional numerical/Monte Carlo reference; full details are deferred to Appendix C.2. Unless stated otherwise, the number of samples is $n_\mu = n_\nu = 10,000$

Family	Scen.	Param.	Ratio $D_{f,\nu}^{(K)}(\mu)$ for $K =$				
			32	64	128	256	512
Mean shift	JS	$\Delta = 0.5$	0.933 ± 0.040	0.968 ± 0.041	0.989 ± 0.042	1.003 ± 0.042	1.013 ± 0.042
		$\Delta = 1.0$	0.928 ± 0.033	0.961 ± 0.034	0.981 ± 0.035	0.992 ± 0.035	0.999 ± 0.035
		$\Delta = 2.0$	0.930 ± 0.008	0.962 ± 0.008	0.981 ± 0.009	0.991 ± 0.009	0.997 ± 0.009
	KL	$\Delta = 0.5$	0.946 ± 0.060	0.987 ± 0.063	1.013 ± 0.065	1.030 ± 0.066	1.044 ± 0.068
		$\Delta = 1.0$	0.880 ± 0.024	0.924 ± 0.025	0.952 ± 0.026	0.969 ± 0.027	0.980 ± 0.027
		$\Delta = 2.0$	0.775 ± 0.010	0.844 ± 0.012	0.895 ± 0.013	0.933 ± 0.015	0.959 ± 0.016
Scale change	KL	$\sigma = 1.2$	0.743 ± 0.063	0.841 ± 0.070	0.908 ± 0.072	0.954 ± 0.072	0.991 ± 0.072
		$\sigma = 1.5$	0.779 ± 0.027	0.872 ± 0.029	0.927 ± 0.030	0.958 ± 0.031	0.977 ± 0.031
		$\sigma = 2.0$	0.803 ± 0.018	0.898 ± 0.020	0.953 ± 0.021	0.982 ± 0.022	0.998 ± 0.022
	Hell^2	$\sigma = 1.2$	0.741 ± 0.077	0.853 ± 0.089	0.931 ± 0.098	0.986 ± 0.106	1.029 ± 0.111
		$\sigma = 1.5$	0.735 ± 0.035	0.842 ± 0.039	0.908 ± 0.041	0.948 ± 0.042	0.973 ± 0.042
		$\sigma = 2.0$	0.744 ± 0.014	0.858 ± 0.014	0.926 ± 0.014	0.965 ± 0.013	0.987 ± 0.012
Multimodal	JS	$\Delta = 0.5$	0.746 ± 0.157	0.849 ± 0.176	0.926 ± 0.189	0.994 ± 0.196	1.068 ± 0.199
	JS	$\Delta = 1.0$	0.769 ± 0.038	0.849 ± 0.040	0.898 ± 0.041	0.929 ± 0.041	0.948 ± 0.042
	JS	$\Delta = 2.0$	0.846 ± 0.019	0.912 ± 0.020	0.950 ± 0.021	0.972 ± 0.021	0.985 ± 0.021
Heavy tails	JS	—	0.488 ± 0.028	0.651 ± 0.036	0.778 ± 0.041	0.869 ± 0.044	0.933 ± 0.046

Table 1: 1D divergence estimation benchmarks (10 runs). We report the ratio estimate/reference (mean \pm std) for various K values. Boldface highlights, for each row, the K whose mean ratio is closest to 1 (i.e., the most accurate approximation)

and results are averaged over 10 seeds. Table 1 reports the ratio $D_{f,\nu}^{(K)}(\mu)/D_{f,\nu}(\mu)$ for $K \in \{32, 64, 128, 256, 512\}$. For the mean shift, the Jensen-Shannon (JS) divergence outperforms the KL, while for the scale change experiments, the KL outperforms the squared Hellinger divergence. Additional figures and sweeps over (n, K) are provided in Section C.2.

4.3 Sliced rank-statistic f -divergences: Empirical convergence

We consider d -dimensional benchmarks using the sliced estimator $D_{f,\nu}^{(K)}(\mu)$, obtained by averaging the one-dimensional rank divergence over L random projections. Unless stated otherwise, $K = 64$, $L = 128$, $n_\mu = n_\nu = 10,000$, and results are reported as mean \pm std over $R = 10$ runs. Implementation details are deferred to Appendix C.3.

Three settings are considered: (i) Gaussian–Gaussian pairs, (ii) covariance mismatches (isotropic and anisotropic), and (iii) non-Gaussian pairs. For (i), KL and squared Hellinger have closed-form references, while JS is approximated by a moment-matched Gaussian proxy. For (iii), reference values are obtained by Monte Carlo evaluation of the divergence formula using closed-form log-densities.

Figure 3 reports the ratio $d D_{f,\nu}^{(K)}(\mu)/D_{f,\nu}(\mu)$ for mean-shift benchmarks across several dimensions. Overall, the ratio stays close to one with moderate variability, indicating that the simple d -scaling provides a reasonable normalization in these settings. Deviations become more noticeable in higher dimension, especially for JS and KL, suggesting that a fixed number of projections L can lead to mild under/over-estimation as d grows, while squared Hellinger remains comparatively stable. Additional benchmarks and ablations are reported in Appendix C.3.

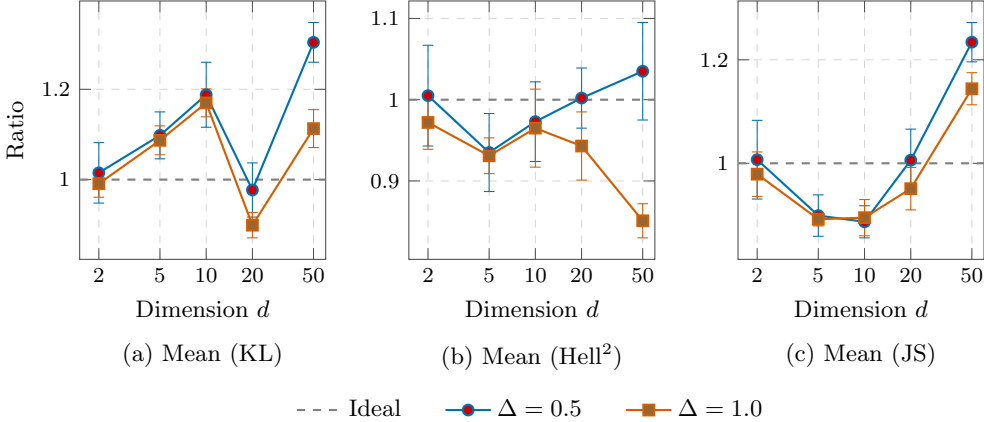


Figure 3: Comparison of mean shift metrics across dimensions for KL, Hellinger, and JS divergences.

4.4 Generative transport dynamics for rank f -divergences

A useful way to turn a discrepancy into a learning principle is to interpret it as an energy and derive an update rule that transports samples in data space toward a target distribution. In our setting, the energy is the (sliced) rank f -divergence, and we implement its minimization through a particle transport dynamics based on one-dimensional quantile matching.

Given particles $\{x_i\}_{i=1}^N \sim \mu$ and reference samples $\{y_j\}_{j=1}^M \sim \nu$, we draw directions $s_1, \dots, s_L \in \mathbb{S}^{d-1}$ and form one-dimensional projections

$$x_i^{(\ell)} := \langle x_i, s_\ell \rangle, \quad y_j^{(\ell)} := \langle y_j, s_\ell \rangle.$$

For each slice ℓ , we compute soft ranks with respect to the reference slice $\nu^{(\ell)} := (s_\ell)_\# \nu$,

$$U_{0,i}^{(\ell)} \approx \hat{R}_{\nu^{(\ell)}}(x_i^{(\ell)}) \in [0, 1], \quad \ell \in \{1, \dots, L\},$$

where $\hat{R}_{\nu^{(\ell)}}$ is the empirical CDF built using the samples $(y_j^{(\ell)})_{j=1}^M$. To update these ranks, we define from any vector $U = (U_1, \dots, U_N) \in [0, 1]^N$ a discrete pmf on $[K]$ via a Bernstein-smoothed histogram (the discretization of $Q_{\mu|\nu}^{(K)}$)

$$\hat{Q}^{(K)}(U)(n) := \frac{1}{N} \sum_{i=1}^N b_{n,K}(U_i), \quad n \in [K]. \quad (6)$$

and we measure its deviation from uniformity exactly as in Definition 2.2:

$$D_f(\hat{Q}^{(K)}(U) \parallel U_K) = \frac{1}{K+1} \sum_{n=0}^K f((K+1)\hat{Q}^{(K)}(U)(n)) \quad (7)$$

We then perform a proximal refinement in rank space:

$$U_1^{(\ell)} \in \arg \min_{U \in [0, 1]^N} \left\{ D_f(\hat{Q}^{(K)}(U) \parallel U_K) + \frac{1}{2\eta} \|U - U_0^{(\ell)}\|_2^2 \right\}, \quad (8)$$

where $\eta > 0$ controls the trust in the current ranks. In practice, (8) can be approximated by deterministic updates (e.g. SGD) or by Langevin-type inner samplers (ULA/MALA).

The updated ranks are mapped back to the projection axis via the empirical quantile of the reference slice,

$$z_i^{(\ell)} \approx \widehat{F}_{\nu^{(\ell)}}^{-1}(U_{1,i}^{(\ell)}), \quad \Delta_i^{(\ell)} := z_i^{(\ell)} - x_i^{(\ell)},$$

which corresponds to a one-dimensional monotone transport correction. Finally, we lift these corrections back to \mathbb{R}^d by aggregating over slices:

$$x_i \leftarrow x_i + \varepsilon \frac{d}{L} \sum_{\ell=1}^L \Delta_i^{(\ell)} s_\ell, \quad (9)$$

with step size $\varepsilon > 0$ (optionally with per-slice clipping for stability). Iterating (9) yields a practical transport dynamics that moves the particle cloud toward ν while being driven by a bounded, rank-based energy. The full pseudocode of the proposed transport algorithm is given in Appendix C.4.

Remark 4.1. This particle algorithm resembles an explicit time discretization of a Wasserstein gradient flow [2, 48] of a Moreau envelope of $D_{f,\nu}^{(K)}$ (similar to [52]), the difference being that here the Moreau envelope is taken in quantile space.

4.4.1 Two-dimensional toy examples

We illustrate the induced particle dynamics on four 2D toy targets: (i) a checkerboard distribution, (ii) a noisy ring, (iii) a two-spirals dataset, and (iv) a two-component Gaussian mixture (two blobs). In each case we draw M reference samples from the target ν and initialize N particles from an isotropic Gaussian. We then iterate (9) for a fixed number of outer steps and report snapshots at $t \in \{0, 1, 5, 10, 20, 40, 100, 200, 400\}$.

Figure 4 uses an SGD approximation of the rank-proximal refinement (8) with the KL generator, $L = 10$ projection directions, and trust-region parameter $\eta = 0.5$. We use a moderate outer step size by starting from $\varepsilon = 0.20$ and linearly annealing it to 0.15 over training; in parallel we anneal the rank smoothing temperature (cf. Algorithm 1) from $\tau = 0.30$ to 0.10 and increase the rank resolution from $K = 80$ to $K = 128$.

Qualitatively, the dynamics rapidly matches the target geometry across very different structures. On the checkerboard, particles populate multiple disconnected cells without degenerating to a single region; on the ring, they expand radially and then redistribute along the angular direction; on spirals, the cloud progressively aligns with the nonlinear manifold; and on the two-blobs mixture, it splits and concentrates around both modes.

4.4.2 CelebA experiments

We next illustrate the induced particle dynamics on *CelebA* using a center-outward rank-proximal transport (CO-RPT) update (see details of the algorithm in Appendix C.4). We treat each particle as a 64×64 RGB image (flattened to $\mathbb{R}^{3 \cdot 4096}$) and use M real images as reference samples from the target distribution ν . Starting from N i.i.d. Gaussian particles, we iterate the center-outward transport update for a fixed number of outer steps (see Section C.5 for full schedules).

In our runs, we use the KL generator with trust parameter $\eta = 0.5$ and a small number of inner prox steps per iteration. We adopt a moderate outer step size by linearly annealing ε from 0.16 to 0.10 over training; in parallel we anneal the rank-smoothing temperature from $\tau = 0.30$ to 0.07

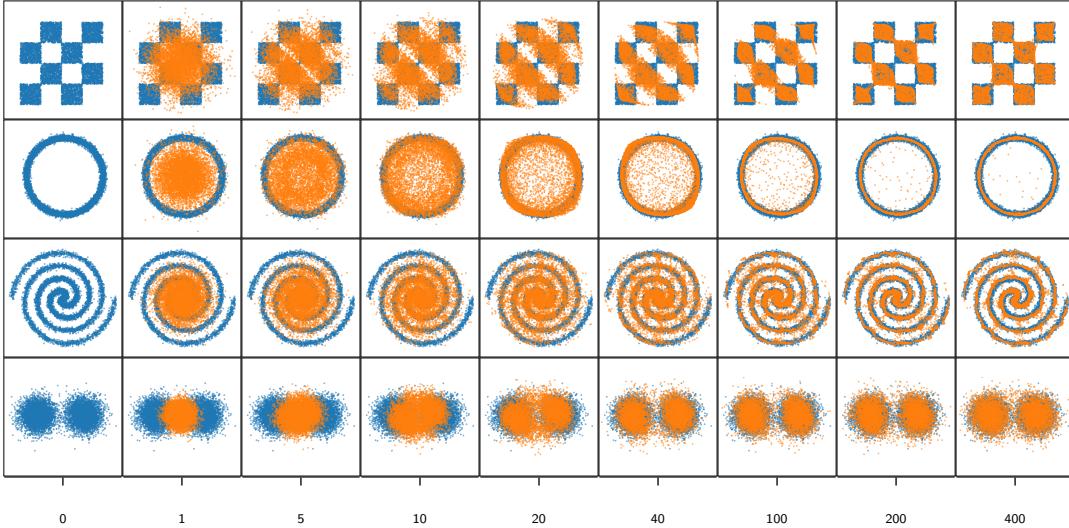


Figure 4: Rank-Proximal Transport on 2D toy targets. Using SGD to minimize the rank-statistic KL with $L = 10$ random projections, particles (orange) evolve from a Gaussian start ($t = 0$) to match the target support (blue).

and increase the rank resolution from $K = 96$ to $K = 224$. To avoid overly large updates in high dimension, we clip the per-particle correction with a cap of 0.30.

Qualitatively, the dynamics progressively transforms the initial noise cloud into structured images that match low- and mid-level statistics of the dataset (global color balance, coarse layout, and face-like contours); see Figure 5. Further implementation details, and qualitative results on MNIST are deferred to Section C.5.

5 Conclusions, future work, and limitations

We proposed *rank-statistic* approximations of f -divergences that replace density-ratio estimation with simple rank counting in a discrete histogram. The resulting surrogate $D_{f,\nu}^{(K)}(\mu)$ has a clean variational structure (convexity and weak lower semicontinuity), is nondecreasing in the resolution K , and remains dominated by the target divergence; under mild regularity of the density ratio we proved consistency as $K \rightarrow \infty$ with quantitative rates, and established finite-sample deviation guarantees for practical estimators. For multivariate data, we introduced sliced rank-statistic divergences by averaging the univariate construction over random 1D projections, inheriting its key properties, and we validated the approach empirically on synthetic benchmarks and as a stable learning objective for implicit generative modelling.

We generalized the rank-statistic approximation of the TV-divergence from [13]. Since the TV-divergence is the only f -divergence which is also an integral probability metric (IPM) [36], it would be interesting to see if IPMs like maximum mean discrepancy [7] or the Wasserstein-1 metric can be approximated by rank-statistics as well. It could be also promising to replace the Bernstein polynomials by another family, like B-splines or general non-linear filters. Investigating the geodesic convexity properties of $D_{f,\nu}^{(K)}$ in the Wasserstein geometry could yield to convergence



Figure 5: CO-RPT samples on CelebA (64×64) after $T = 20,000$ outer steps.

rates of the generative transport dynamics. Lastly, it would be interesting to find an a joint regime for $(K, N) \rightarrow \infty$ yielding the best convergence rate. All of these questions are currently being undertaken by the authors.

Our results also highlight limitations: projection complexity in high dimensions when discrepancies are strongly anisotropic or concentrated in dependencies that are hard to detect from 1D views, and the reliance on random directions for capturing such effects efficiently. Future work includes variance-reduced and structured projection schemes (e.g., orthogonal or quasi-Monte Carlo directions), improved anisotropy calibration beyond simple $d \times$ normalizations, tighter dimension-dependent guarantees, and scaling the objective inside modern large-scale generative pipelines. We expand the discussion of limitations and future directions in Appendix D.

Acknowledgments. V. Stein and J.M. de Frutos thank their respective advisors, Gabriele Steidl and Joaquín Míguez, for their invaluable support and guidance throughout this work. V. Stein furthermore thanks Joaquín Míguez for the invitation to uc3m in November 2025.



This project has received funding from the European Research Council (ERC) under the European Union's Horizon Europe research and innovation programme (grant agreement No. 101198055, project acronym NEITALG). This work has also been partially supported by the Office of Naval Research (award N00014-22-1-2647) and Spain's Agencia Estatal de Investigación (ref. PID2024-158181NB-I00 NISA and PID2021-123182OB-I00 EPICENTER) funded by MCIN/AEI/10.13039/501100011033 and by "ERDF A way of making Europe."

Views and opinions expressed are however those of the author(s) only and do not necessarily reflect those of the European Union, the European Research Council Executive Agency, the U.S. Office of Naval Research, or the Spanish Agencia Estatal de Investigación. Neither the European Union nor any of the aforementioned granting authorities can be held responsible for them.

References

- [1] S. M. Ali and S. D. Silvey. A general class of coefficients of divergence of one distribution from another. *Journal of the Royal Statistical Society: Series B (Methodological)*, 28(1):131–142, 1966.
- [2] L. Ambrosio, N. Gigli, and G. Savaré. *Gradient flows: in metric spaces and in the space of probability measures*. Springer Science & Business Media, 2 edition, 2008.
- [3] M. Arjovsky, S. Chintala, and L. Bottou. Wasserstein generative adversarial networks. In *International Conference on Machine Learning*, pages 214–223. PMLR, 2017.
- [4] M. Beckmann, R. Beinert, and J. Bresch. Max-normalized Radon cumulative distribution transform for limited data classification. In *International Conference on Scale Space and Variational Methods in Computer Vision (SSVM)*, volume 15667 of *Lect. Notes Comput. Sci.*, pages 241–254, Cham, Switzerland, 2025. Springer.
- [5] M. I. Belghazi, A. Baratin, S. Rajeshwar, S. Ozair, Y. Bengio, A. Courville, and D. Hjelm. Mutual information neural estimation. In *International Conference on Machine Learning*, pages 531–540. PMLR, 2018.
- [6] S. Bernstein. Démonstration du théorème de Weierstrass fondée sur le calcul des probabilités. *Communications of the Kharkiv Mathematical Society*, 13(1):1–2, 1912.
- [7] K. M. Borgwardt, A. Gretton, M. J. Rasch, H.-P. Kriegel, B. Schölkopf, and A. J. Smola. Integrating structured biological data by kernel maximum mean discrepancy. *Bioinformatics*, 22(14):e49–e57, 07 2006.
- [8] S. Boucheron, G. Lugosi, and P. Massart. *Concentration Inequalities: A Nonasymptotic Theory of Independence*. Oxford Series in Probability and Its Applications. Oxford University Press, Oxford, UK, 2nd edition, 2016.

- [9] J. Choi and B. Han. MCL-GAN: Generative adversarial networks with multiple specialized discriminators. *Advances in Neural Information Processing Systems*, 35:29597–29609, 2022.
- [10] I. Csiszár. On information-type measure of difference of probability distributions and indirect observations. *Studia Scientiarum Mathematicarum Hungarica*, 2:299–318, 1967.
- [11] J. M. de Frutos, P. M. Olmos, M. A. V. Lopez, and J. Míguez. Training implicit generative models via an invariant statistical loss. In *International Conference on Artificial Intelligence and Statistics*, pages 2026–2034. PMLR, 2024.
- [12] J. M. de Frutos, M. A. Vázquez, P. Olmos, and J. Míguez. Robust training of implicit generative models for multivariate and heavy-tailed distributions with an invariant statistical loss. arXiv preprint arXiv:2410.22381, 2024.
- [13] J. M. de Frutos, M. A. Vázquez, P. M. Olmos, and J. Míguez. Explicit density approximation for neural implicit samplers using a Bernstein-based convex divergence. In *International Conference on Artificial Intelligence and Statistics*, page tbd. PMLR, 2026.
- [14] I. Deshpande, Y.-T. Hu, R. Sun, A. Pyrros, N. Siddiqui, S. Koyejo, Z. Zhao, D. Forsyth, and A. G. Schwing. Max-sliced Wasserstein distance and its use for GANs. In *Proceedings of the IEEE/CVF Conference on Computer Vision and Pattern Recognition*, pages 10648–10656, 2019.
- [15] J. Dick and F. Pillichshammer. *Digital nets and sequences: discrepancy theory and quasi-Monte Carlo integration*. Cambridge University Press, 2010.
- [16] I. Durugkar, I. Gemp, and S. Mahadevan. Generative multi-adversarial networks. *arXiv preprint arXiv:1611.01673*, 2016.
- [17] V. Elvira, J. Miguez, and P. M. Djurić. On the performance of particle filters with adaptive number of particles. *Statistics and Computing*, 31(6):81, 2021.
- [18] T. Gneiting, F. Balabdaoui, and A. E. Raftery. Probabilistic forecasts, calibration and sharpness. *Journal of the Royal Statistical Society Series B: Statistical Methodology*, 69(2):243–268, 2007.
- [19] I. J. Goodfellow, J. Pouget-Abadie, M. Mirza, B. Xu, D. Warde-Farley, S. Ozair, A. Courville, and Y. Bengio. Generative adversarial nets. *Advances in Neural Information Processing Systems*, 27, 2014.
- [20] I. Gulrajani, F. Ahmed, M. Arjovsky, V. Dumoulin, and A. C. Courville. Improved training of Wasserstein GANs. *Advances in Neural Information Processing Systems*, 30, 2017.
- [21] M. Gutmann and A. Hyvärinen. Noise-contrastive estimation: A new estimation principle for unnormalized statistical models. In *Proceedings of the Thirteenth International Conference on Artificial Intelligence and Statistics*, pages 297–304. JMLR Workshop and Conference Proceedings, 2010.
- [22] T. M. Hamill. Interpretation of rank histograms for verifying ensemble forecasts. *Monthly Weather Review*, 129(3):550–560, 2001.
- [23] H. Knothe. Contributions to the theory of convex bodies. *Michigan Mathematical Journal*, 4(1):39–52, 1957.

- [24] S. Kolouri, K. Nadjahi, U. Simsekli, R. Badeau, and G. Rohde. Generalized sliced Wasserstein distances. *Advances in Neural Information Processing Systems*, 32, 2019.
- [25] S. Kolouri, K. Nadjahi, U. Simsekli, R. Badeau, and G. Rohde. Generalized sliced Wasserstein distances. In *Advances in Neural Information Processing Systems*, volume 32, 2019.
- [26] A. Kontorovich. On the tensorization of the variational distance. *Electronic Communications in Probability*, 30:1–10, 2025.
- [27] A. Kontorovich. TV homogenization inequalities. arXiv preprint arXiv:2601.04079, 2026.
- [28] A. Leblanc. On estimating distribution functions using bernstein polynomials. *Annals of the Institute of Statistical Mathematics*, 64(5):919–943, 2012.
- [29] J. Lin. Divergence measures based on the Shannon entropy. *IEEE Transactions on Information Theory*, 37(1):145–151, 1991.
- [30] B. G. Lindsay. Efficiency versus robustness: The case for minimum Hellinger distance and related methods. *The Annals of Statistics*, 22(2):1081 – 1114, 1994.
- [31] Z. Liu, P. Luo, X. Wang, and X. Tang. Deep learning face attributes in the wild. In *Proceedings of International Conference on Computer Vision (ICCV)*, December 2015.
- [32] A. Liutkus, U. Simsekli, S. Majewski, A. Durmus, and F.-R. Stöter. Sliced-Wasserstein flows: Nonparametric generative modeling via optimal transport and diffusions. In *International Conference on machine learning*, pages 4104–4113. PMLR, 2019.
- [33] G. G. Lorentz. *Bernstein polynomials*. Chelsea Publishing Company, New York, N.Y., 2nd edition, 1968.
- [34] P. Massart. The tight constant in the Dvoretzky-Kiefer-Wolfowitz inequality. *The Annals of Probability*, pages 1269–1283, 1990.
- [35] K. R. Moon and A. O. Hero. Multivariate f -divergence estimation with confidence. *Advances in Neural Information Processing Systems*, 27, 2014.
- [36] A. Müller. Integral probability metrics and their generating classes of functions. *Advances in applied probability*, 29(2):429–443, 1997.
- [37] K. Nadjahi, A. Durmus, L. Chizat, S. Kolouri, S. Shahrampour, and U. Simsekli. Statistical and topological properties of sliced probability divergences. *Advances in Neural Information Processing Systems*, 33:20802–20812, 2020.
- [38] X. Nguyen, M. J. Wainwright, and M. I. Jordan. Estimating divergence functionals and the likelihood ratio by convex risk minimization. *IEEE Transactions on Information Theory*, 56(11):5847–5861, 2010.
- [39] S. Nietert, Z. Goldfeld, R. Sadhu, and K. Kato. Statistical, robustness, and computational guarantees for sliced Wasserstein distances. In *Advances in Neural Information Processing Systems*, volume 35, pages 28179–28193, 2022.

[40] S. Nowozin, B. Cseke, and R. Tomioka. *f*-GAN: Training generative neural samplers using variational divergence minimization. *Advances in Neural Information Processing Systems*, 29, 2016.

[41] F.-P. Paty and M. Cuturi. Subspace robust Wasserstein distances. In *International conference on machine learning*, pages 5072–5081. PMLR, 2019.

[42] Y. Polyanskiy and Y. Wu. *Information theory: From coding to learning*. Cambridge university press, 2025.

[43] A. Radford, L. Metz, and S. Chintala. Unsupervised representation learning with deep convolutional generative adversarial networks. arxiv 2015. *arXiv preprint arXiv:1511.06434*, 5, 2015.

[44] M. Rosenblatt. Remarks on a multivariate transformation. *The Annals of Mathematical Statistics*, 23(3):470–472, 1952.

[45] P. Rubenstein, O. Bousquet, J. Djolonga, C. Riquelme, and I. O. Tolstikhin. Practical and consistent estimation of *f*-divergences. *Advances in Neural Information Processing Systems*, 32, 2019.

[46] A. Ruderman, M. Reid, D. García-García, and J. Petterson. Tighter variational representations of *f*-divergences via restriction to probability measures. arXiv preprint arXiv:1206.4664, 2012.

[47] M. S. Sajjadi, O. Bachem, M. Lucic, O. Bousquet, and S. Gelly. Assessing generative models via precision and recall. *Advances in Neural Information Processing Systems*, 31, 2018.

[48] F. Santambrogio. {Euclidean, metric, and Wasserstein} gradient flows: an overview. *Bulletin of Mathematical Sciences*, 7(1):87–154, 2017.

[49] I. R. Savage. A note on non-parametric methods. Technical report, U.S. Department of Commerce National Bureau of Standards, 1952. NBS project 1103-11-1107, NBS report 1699.

[50] I. M. Sobol. Distribution of points in a cube and approximate evaluation of integrals. *USSR Computational Mathematics and Mathematical Physics*, 7:86–112, 1967.

[51] S. Sreekumar, Z. Zhang, and Z. Goldfeld. Non-asymptotic performance guarantees for neural estimation of *f*-divergences. In *International Conference on Artificial Intelligence and Statistics*, pages 3322–3330. PMLR, 2021.

[52] V. Stein, S. Neumayer, N. Rux, and G. Steidl. Wasserstein gradient flows for Moreau envelopes of *f*-divergences in reproducing kernel Hilbert spaces. *Analysis and Applications*, 24(01):21–65, 2026.

[53] A. W. van der Vaart and J. A. Wellner. *Weak Convergence and Empirical Processes: With Applications to Statistics*. Springer Series in Statistics. Springer, New York, 1996.

[54] J. Wu, Z. Huang, D. Acharya, W. Li, J. Thoma, D. P. Paudel, and L. V. Gool. Sliced Wasserstein generative models. In *Proceedings of the IEEE/CVF Conference on Computer Vision and Pattern Recognition*, pages 3713–3722, 2019.

Appendix

In this appendix, we first recall well-known results about Bernstein polynomials and f -divergences in Section A. In Section B we prove the theorems from the main text, and in Section C we provide supplementary explanations and experiments. Finally, in Section D, we elaborate on limitations and future work.

A Well-known results

Here, we recall results about Bernstein polynomials and f -divergences.

Bernstein polynomials were introduced in [6] to prove the Weierstraß approximation theorem in a simple way.

Lemma A.1 (Properties of Bernstein polynomials). *The Bernstein polynomials $b_{n,K} : [0, 1] \rightarrow [0, \infty)$, $u \mapsto \binom{K}{n} u^n (1-u)^{K-n}$ have the following properties.*

1. We have $\sum_{n=0}^K b_{n,K}(s) = 1$ for all $s \in [0, 1]$, and $\int_0^1 b_{n,K}(s) \, ds = \frac{1}{K+1}$ for $n \in [K]$.
2. For $K \in \mathbb{N}$ and $n \in [K-1]$ we have

$$b_{n,K-1} = \frac{K-n}{K} b_{n,K} + \frac{n+1}{K} b_{n+1,K}.$$

3. The function $(K+1)b_{n,K}$ is the probability density function of the Beta($n+1, K-n+1$) distribution, whose mean and variance are $\frac{n+1}{K+2}$ and $\frac{(n+1)(K-n+1)}{(K+2)^2(K+3)}$, respectively.
4. Let $f \in \mathcal{C}([0, 1])$. For the Bernstein operator $B_K : \mathcal{C}([0, 1]; \mathbb{R}) \rightarrow \Pi_K$, $f \mapsto \sum_{n=0}^K f\left(\frac{n}{K}\right) b_{n,K}$ we have $\|B_K[f] - f\|_\infty \rightarrow 0$ for $K \rightarrow \infty$.
5. If g is Lipschitz, then $\|B_K[g] - g\|_\infty \in O(K^{-\frac{1}{2}})$ and if $g \in \mathcal{C}^2([0, 1])$, then $\|B_K[g] - g\|_\infty \in O(K^{-1})$.

Proof. See [33, Chp. 1]. □

Lemma A.2 (Data processing inequality for discrete f -divergences). *For finite sets X and Y and a matrix $W \in [0, 1]^{\#Y \times \#X}$ fulfilling $W \mathbf{1}_{\#Y} = \mathbf{1}_{\#X}$ and $P, Q \in \mathcal{P}(X)$ we have*

$$D_f(W^\top P \mid W^\top Q) \leq D_f(P \mid Q).$$

Proof. See [42, Subsec. 7.2]. □

B Proofs of theorems

First, we repeat some important properties of the rank statistics [11, App. A] [13, Thm. 4.1].

B.1 Properties of the rank statistic

Lemma B.1 (Properties of the rank statistic). *Let $\mu, \nu \in \mathcal{P}(\mathbb{R})$ with $\mu \ll \nu$ and $K \in \mathbb{N}_{>0}$, and let $(b_{n,K})_{n \in [K]}$ be the Bernstein polynomials.*

1. *We have*

$$Q_{\mu|\nu}^{(K)}(n) = \int_{\mathbb{R}} b_{n,K}(R_{\nu}(y)) d\mu(y) = \int_0^1 b_{n,K}(s) \left(\frac{d\mu}{d\nu} \circ Q_{\nu} \right)(s) ds, \quad \forall n \in [K], \quad (10)$$

where R_{ν} and Q_{ν} are the cumulative distribution function (CDF) and the quantile function of ν , respectively.

2. *Furthermore, we have $\mu = \nu$ if and only if for all $K \in \mathbb{N}$ we have $A_{\mu|\nu}^{(K)} \sim U_K$, i.e., $Q_{\mu|\nu}^{(K)}(n) = \frac{1}{K+1}$ for all $n \in [K]$.*

Proof. 1. Given $y \sim \mu$, the random variable $A_{\mu|\nu}^{(K)} | y$ follows a $\text{Bin}(K, R_{\nu}(y))$ distribution, whose probability mass function is $[K] \ni n \mapsto b_{n,K}(R_{\nu}(y))$. By the law of total probability, we thus have

$$Q_{\mu|\nu}^{(K)}(n) = \mathbb{P}(A_{\mu|\nu}^{(K)} = n) = \int_{\mathbb{R}} \mathbb{P}(A_{\mu|\nu}^{(K)} = n | y) d\mu(y) = \int_{\mathbb{R}} (b_{n,K} \circ R_{\nu})(y) d\mu(y)$$

as in [17, Eq. (B.2)]. The second equation follows from the change of variables formula for the pushforward measure.

2. If $\mu = \nu$ and $K \in \mathbb{N}$, then

$$Q_{\mu|\nu}^{(K)}(n) = \int_0^1 b_{n,K}(s) \left(\frac{d\mu}{d\nu} \circ Q_{\nu} \right)(s) ds = \int_0^1 b_{n,K}(s) ds = \frac{1}{K+1}, \quad \forall n \in [K].$$

The converse direction follows like in the proof of [11, Thm. 3], the assumption that μ and ν admit densities is not needed. \square

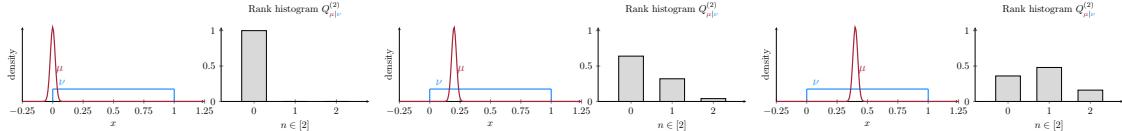


Figure 6: Illustration of the rank histogram $Q_{\mu|\nu}^{(K)}$ for $K = 2$, $\nu \sim U([0, 1])$ and μ being a Gaussian with varying mean.

In the next remark, we illustrate why measuring the deviation of the rank histogram $Q_{\mu|\nu}^{(K)}$ using an f -divergence is meaningful.

Remark B.2 (Suitability of f -divergences). For $\mu, \nu \in \mathcal{P}(\mathbb{R})$ with $\mu \ll \nu$, we have

$$D_{f,\nu}(\mu) = \int_{\mathbb{R}} f \left(\frac{d\mu}{d\nu}(x) \right) d[Q_{\nu} \# \lambda_{(0,1)}](x) = \int_0^1 f \left(\left(\frac{d\mu}{d\nu} \circ Q_{\nu} \right)(s) \right) ds = D_{f,\lambda_{(0,1)}} \left(\frac{d\mu}{d\nu} \circ Q_{\nu} \cdot \lambda_{(0,1)} \right),$$

where $\lambda_{(0,1)}$ is the Lebesgue measure on $(0, 1)$. Hence, the f -divergence between μ and ν can be rewritten as the f -divergence between two densities on the (bounded) unit interval. The same holds for the α -Rényi divergences, and we leave the exploration of rank-statistic approximations of Rényi divergences for future work.

This clean reformulation is not possible for other discrepancies, like integral probability metrics or Wasserstein distances.

B.2 Proof of Theorem 2.3

Theorem 2.3. *Let $\mu, \nu \in \mathcal{P}(\mathbb{R})$ and $K \in \mathbb{N}$. The map $D_{f,\nu}^{(K)}$ is convex and if Q_ν is continuous, it is also weakly lower semicontinuous. Furthermore,*

$$D_{f,\nu}^{(K)}(\mu) \leq D_{f,\nu}^{(K+1)}(\mu) \leq D_{f,\nu}(\mu). \quad (3)$$

Proof. 1. First, we show that $D_{f,\nu}^{(K)} \leq D_{f,\nu}$.

Let $U_{n,K} \sim \text{Beta}(n+1, K-n+1)$ and $r := \frac{d\mu}{d\nu} \circ Q_\nu$. Then,

$$c_n^{(K)} := (K+1) Q_{\mu|\nu}^{(K)}(n) = \int_0^1 (K+1) b_{n,K}(u) r(u) \, du = \mathbb{E}[r(U_{n,K})],$$

By Jensen's inequality, we have

$$\begin{aligned} D_f^{(K)}(\mu | \nu) &= \frac{1}{K+1} \sum_{n=0}^K f(c_n^{(K)}) \leq \frac{1}{K+1} \sum_{n=0}^K \mathbb{E}[f(r(U_{n,K}))] \\ &= \frac{1}{K+1} \sum_{n=0}^K \int_0^1 f(r(u))(K+1) b_{n,K}(u) \, du = \int_0^1 f(r(u)) \, du, \end{aligned}$$

where in the last step we used $\frac{1}{K+1} \sum_{n=0}^K (K+1) b_{n,K} \equiv 1$.

2. Now, we prove the monotonicity with respect to K .

We want to use the data-processing inequality for discrete f -divergences (Lemma A.2) with $X := [K+1]$, $Y := [K]$, $P := Q_{\mu|\nu}^{(K+1)}$, and $Q := \mathcal{U}([K+1])$ and construct W such that $W^\top P = Q_{\mu|\nu}^{(K+1)}$ and $W^\top Q = U_K$. Then,

$$\begin{aligned} D_{f,\nu}^{(K)}(\mu) &= D_f(Q_{\mu|\nu}^{(K)} | U_K) = D_f(Q_{\mu|\nu}^{(K+1)} W | U_{K+1} W) \\ &\leq D_f(Q_{\mu|\nu}^{(K+1)} \| U_{K+1}) = D_{f,\nu}^{(K+1)}(\mu). \end{aligned}$$

We set

$$W_{n,m} := \begin{cases} \frac{m}{K+1}, & \text{if } n = m-1, \\ \frac{K+1-m}{K+1}, & \text{if } n = m, \\ 0, & \text{otherwise.} \end{cases} \quad n \in [K], m \in [K+1].$$

Then,

$$\begin{aligned} W \mathbf{1}_{K+1} &= \left(\sum_{n=0}^K W_{n,m} \right)_{m \in [K+1]} = (W_{m-1,m} + W_{m,m})_{m \in [K+1]} \\ &= \left(\frac{m}{K+1} + \frac{K+1-m}{K+1} \right)_{m \in [K+1]} = \mathbf{1}_{K+2} \end{aligned}$$

and

$$\begin{aligned} W^\top Q &= W^\top \mathcal{U}([K+1]) = \left(\sum_{m=0}^K W_{n,m} \frac{1}{K+2} \right)_{n \in [K]} = \left(\frac{1}{K+2} (W_{n,n} + W_{n,n+1}) \right)_{n \in [K]} \\ &= \frac{1}{K+2} \left(\frac{K+1-n}{K+1} + \frac{n+1}{K+1} \right)_{n \in [K]} = \frac{1}{K+1} \mathbf{1}_{K+1} = U_K. \end{aligned}$$

Next,

$$\begin{aligned} W^\top P &= W^\top Q_{\mu|\nu}^{(K+1)} = \left(W_{n,n} Q_{\mu|\nu}^{(K+1)}(n) + W_{n,n+1} Q_{\mu|\nu}^{(K+1)}(n+1) \right)_{n \in [K]} \\ &= \left(\frac{K+1-n}{K+1} \int_{\mathbb{R}} b_{n,K+1} \circ R_\nu \, d\mu + \frac{n+1}{K+1} \int_{\mathbb{R}} b_{n,K+1} \circ R_\nu \, d\mu \right)_{n \in [N]} \\ &= \left(\int_{\mathbb{R}} b_{n,K} \circ R_\nu \, d\mu \right)_{n \in [K]} = Q_{\mu|\nu}^{(K)}. \end{aligned}$$

The identity about Bernstein polynomials we use in the last line expresses that starting from a count n of “successes” among $K+1$ trials (n of the $K+1$ samples that are drawn from ν are lower than $Y \sim \mu$), we delete one trial uniformly at random. With probability $n/(K+1)$ we delete a success and the new count is $n-1$, while with probability $(K+1-n)/(K+1)$ we delete a failure and the new count remains n .

3. By (10), $Q_{\mu|\nu}^{(K)}(n)$ is linear in μ . Since f is convex, the functional $D_{f,\nu}^{(K)}$ is convex as well.
4. If Q_ν is continuous, then by (10), $Q_{\mu|\nu}^{(K)}$ is weakly continuous, since the integrand is continuous. Hence, $D_{f,\nu}^{(K)}$ is weakly lower semicontinuous by the lower semicontinuity of f . \square

B.3 Proof of Theorem 2.5

First, we prove the convergence if $r \in \mathcal{C}([0, 1])$.

Proof. The only thing not proved in proof sketch in the main text is the uniform convergence of r_K to r for $K \rightarrow \infty$.

Indeed, for $u \in \left[\frac{n}{K+1}, \frac{n+1}{K+1} \right)$ we have

$$|r_K(u) - r(u)| = \left| c_n^{(K)} - r(u) \right| \leq \left| c_n^{(K)} - r\left(\frac{n}{K}\right) \right| + \left| r\left(\frac{n}{K}\right) - r(u) \right|.$$

The second summand is bounded above as follows:

$$\left| r\left(\frac{n}{K}\right) - r(u) \right| \leq \sup \left\{ |r(x) - r(y)| : |x - y| \leq \frac{1}{K+1} \right\}, =: \omega_r \left(\frac{1}{K+1} \right),$$

which is the *modulus of continuity* of r at $\frac{1}{K+1}$. Hence,

$$\|r_K - r\|_\infty \leq \max_{n \in [K]} \left| c_n^{(K)} - r\left(\frac{n}{K}\right) \right| + \omega_r \left(\frac{1}{K+1} \right). \quad (11)$$

Since r is uniformly continuous, the second summand vanishes for $K \rightarrow \infty$.

We now upper bound the second summand. Let $U_{n,K} \sim \text{Beta}(n+1, K+1-n)$. The density of $U_{n,K}$ is $(K+1)b_{n,K}$ and its mean is $m_{n,K} := \frac{n+1}{K+2}$. For $n \in [K]$, we have

$$\left| \mathbb{E}[r(U_{n,K})] - r\left(\frac{n}{K}\right) \right| \leq \mathbb{E}[|r(U_{n,K}) - m_{n,K}|] + \left| r(m_{n,K}) - r\left(\frac{n}{K}\right) \right|.$$

Furthermore,

$$\left| m_{n,K} - \frac{n}{K} \right| = \left| \frac{K-2n}{K(K+2)} \right| \leq \frac{1}{K+2} < \frac{1}{K} \rightarrow 0, \quad K \rightarrow \infty, \quad (12)$$

We have

$$\mathbb{V}[U_{n,K}] = \frac{(n+1)(K-n+1)}{(K+2)^2(K+3)} \leq \frac{1}{4(K+3)} < \frac{1}{K}. \quad (13)$$

If the modulus of continuity ω_r is concave, then by Jensen's inequality, we have

$$\begin{aligned} \left| \mathbb{E}[r(U_{n,K})] - r\left(\frac{n}{K}\right) \right| &\leq \mathbb{E}\left[\left| r(U_{n,K}) - r\left(\frac{n}{K}\right) \right| \right] \leq \mathbb{E}\left[\omega_r\left(U_{n,K} - \frac{n}{K}\right) \right] \\ &\leq \omega_r\left(\mathbb{E}\left[\left| U_{n,K} - \frac{n}{K} \right| \right]\right) \leq \omega_r\left(\frac{1}{K+2} + \frac{1}{2\sqrt{K+3}}\right), \end{aligned}$$

where we use Equations (12) and (13) in the last inequality. Hence, by (11),

$$\|r_K - r\|_\infty \leq \omega_r\left(\frac{1}{K+2} + \frac{1}{2\sqrt{K+3}}\right) + \omega_r\left(\frac{1}{K+1}\right) \xrightarrow{K \rightarrow \infty} 0. \quad \square$$

Now, let us prove the convergence rates.

Lemma B.3. *If f is Lipschitz on $\text{ran}(r)$, then*

$$D_{f,\nu}(\mu) - D_{f,\nu}^{(K)} \in \begin{cases} O(K^{-\frac{\alpha}{2}}), & \text{if } r \in C^{0,\alpha}([0, 1]), \\ O(K^{-1}), & \text{if } r \in C^2([0, 1]), \text{ or if } r \text{ is Lipschitz, } f \in C^2([0, \infty)). \end{cases}$$

Proof. 1. If r is H_r -Hölder continuous with exponent $\alpha \in (0, 1]$, then $\omega_r(\delta) = H_r \delta^\alpha$, so the bound becomes

$$D_{f,\nu}(\mu) - D_{f,\nu}^{(K)}(\mu) \leq L_f H_r \left(\left(\frac{1}{K+2} + \frac{1}{2\sqrt{K+1}} \right)^\alpha + \left(\frac{1}{K+1} \right)^\alpha \right).$$

2. If $r \in C^2([0, 1])$. By Taylor's theorem, there exists a ξ between $U_{n,K}$ and $\frac{n}{K}$ such that

$$r(U_{n,K}) = r\left(\frac{n}{K}\right) + r'\left(\frac{n}{K}\right)(U_{n,K} - \frac{n}{K}) + \frac{1}{2}r''(\xi)\left(U_{n,K} - \frac{n}{K}\right)^2,$$

so that

$$\left|c_K(n) - r\left(\frac{n}{K}\right)\right| \leq \|r'\|_\infty \left|m_{n,K} - \frac{n}{K}\right| + \frac{1}{2}\|r''\|_\infty \mathbb{E}\left[(U_{n,K} - \frac{n}{K})^2\right],$$

so by the estimates from Equations (12) and (13) we obtain again

$$\max_{n \in [K]} \left|c_K(n) - r\left(\frac{n}{K}\right)\right| \leq \frac{\|r'\|_\infty}{K+2} + \frac{\|r''\|_\infty}{8(K+3)} + \frac{\|r''\|_\infty}{2(K+2)^2}.$$

Combined with $\omega_r\left(\frac{1}{K+1}\right) \leq \frac{\|r'\|_\infty}{K+1}$, we obtain $\|r_K - r\|_\infty \in O(K^{-1})$.

3. Now assume that r is L_r -Lipschitz and $f \in C^2$ with $\|f''\|_\infty \leq M_f$. For brevity, set

$$Z_{n,K} := r(U_{n,K}), \quad m_{n,K} := \mathbb{E}[Z_{n,K}].$$

By Taylor's theorem with remainder, for every $x \in \mathbb{R}$ there exists ξ_x on the line segment between x and $m_{n,K}$ such that

$$f(x) = f(m_{n,K}) + f'(m_{n,K})(x - m_{n,K}) + \frac{1}{2}f''(\xi_x)(x - m_{n,K})^2.$$

Hence,

$$|f(x) - f(m_{n,K}) - f'(m_{n,K})(x - m_{n,K})| \leq \frac{M_f}{2}(x - m_{n,K})^2.$$

Applying this Taylor expansion with $x = Z_{n,K}$, and using that $m_{n,K} = \mathbb{E}[Z_{n,K}]$ together with the bound $|f''| \leq M_f$ on the remainder, we obtain

$$\begin{aligned} J_{n,K} &= \mathbb{E}[f(Z_{n,K})] - f(\mathbb{E}[Z_{n,K}]) = \mathbb{E}[f(Z_{n,K}) - f(m_{n,K})] \\ &= \mathbb{E}[f(Z_{n,K}) - f(m_{n,K}) - f'(m_{n,K})(Z_{n,K} - m_{n,K}) + f'(m_{n,K})(Z_{n,K} - m_{n,K})] \\ &= \mathbb{E}[f(Z_{n,K}) - f(m_{n,K}) - f'(m_{n,K})(Z_{n,K} - m_{n,K})] + f'(m_{n,K}) \mathbb{E}[Z_{n,K} - m_{n,K}] \\ &= \mathbb{E}[f(Z_{n,K}) - f(m_{n,K}) - f'(m_{n,K})(Z_{n,K} - m_{n,K})] \\ &\leq \mathbb{E}[|f(Z_{n,K}) - f(m_{n,K}) - f'(m_{n,K})(Z_{n,K} - m_{n,K})|] \\ &\leq \frac{M_f}{2} \mathbb{E}[(Z_{n,K} - m_{n,K})^2] = \frac{M_f}{2} \mathbb{V}(Z_{n,K}). \end{aligned}$$

$|r(u) - r(v)| \leq L_r|u - v|$. Using the characterization

$$\mathbb{V}(Z_{n,K}) = \inf_{c \in \mathbb{R}} \mathbb{E}[(Z_{n,K} - c)^2],$$

and taking $c = r(\mathbb{E}[U_{n,K}])$, we get

$$\begin{aligned} \mathbb{V}(Z_{n,K}) &= \inf_{c \in \mathbb{R}} \mathbb{E}[(r(U_{n,K}) - c)^2] \\ &\leq \mathbb{E}[(r(U_{n,K}) - r(\mathbb{E}[U_{n,K}]))^2] \leq L_r^2 \mathbb{E}[(U_{n,K} - \mathbb{E}[U_{n,K}])^2] = L_r^2 \mathbb{V}(U_{n,K}). \end{aligned}$$

Combining the two bounds yields

$$J_{n,K} \leq \frac{M_f}{2} L_r^2 \mathbb{V}(U_{n,K}).$$

As in (13), for $U_{n,K} \sim \text{Beta}(n+1, K-n+1)$ we have $\mathbb{V}(U_{n,K}) < \frac{1}{K}$. Hence

$$J_{n,K} \leq \frac{M_f}{2} L_r^2 \frac{1}{K} = \frac{M_f L_r^2}{2K}.$$

Finally, averaging over n ,

$$0 \leq D_{f,\nu}(\mu) - D_{f,\nu}^{(K)}(\mu) = \frac{1}{K+1} \sum_{n=0}^K J_{n,K} \leq \frac{1}{K+1} \sum_{n=0}^K \frac{M_f L_r^2}{2K} = \frac{M_f L_r^2}{2K}. \quad \square$$

B.4 Proof of Theorem 3.2

Theorem 3.2. *The map $D_{f,\nu}^{(K)}$ is convex. Let $\mu, \nu \in \mathcal{P}(\mathbb{R}^d)$ with $\mu \ll \nu$. Then,*

$$D_{f,\nu}^{(K)}(\mu) \leq \text{SD}_{f,\nu}(\mu) \leq D_{f,\nu}(\mu), \quad K \in \mathbb{N}. \quad (5)$$

If $r_{\mu_s|\nu_s} \in \mathcal{C}([0, 1])$ for almost all $s \in \mathbb{S}^{d-1}$, then

$$\lim_{K \rightarrow \infty} D_{f,\nu}^{(K)}(\mu) = \text{SD}_{f,\nu}(\mu),$$

Proof. The convexity follows like in the proof of Theorem 2.3, because the pushforward is a linear operation. First, note that the absolute continuity $\mu \ll \nu$ implies that the projected measures satisfy $\mu_s \ll \nu_s$ for all $s \in \mathbb{S}^{d-1}$. By Theorem 2.5 we have the direction-wise convergence $\lim_{K \rightarrow \infty} D_{f,\nu_s}^{(K)}(\mu_s) = D_{f,\nu_s}(\mu_s)$. By Theorem 2.3 and by applying the data-processing inequality for f -divergences to the measurable map $x \mapsto s^\top x$, we have $D_{f,\nu_s}^{(K)}(\mu_s) \leq \text{SD}_{f,\nu_s}(\mu_s) \leq D_{f,\nu}(\mu)$. Integrating over the sphere yields (5). Furthermore, we can thus apply the dominated convergence theorem and obtain

$$\lim_{K \rightarrow \infty} \int_{\mathbb{S}^{d-1}} D_{f,\nu_s}^{(K)}(\mu_s) d\sigma(s) = \int_{\mathbb{S}^{d-1}} \lim_{K \rightarrow \infty} D_{f,\nu_s}^{(K)}(\mu_s) d\sigma(s) = \int_{\mathbb{S}^{d-1}} D_{f,\nu_s}(\mu_s) d\sigma(s). \quad \square$$

B.5 Proof of Theorem 2.6

Lemma B.4 (Sampling μ only). *Fix $\nu \in \mathcal{P}(\mathbb{R})$ and $K \in \mathbb{N}$. Let $\mu \in \mathcal{P}(\mathbb{R})$ and let $\hat{\mu}_N$ be the empirical measure based on N i.i.d. samples from μ . Then, denoting $\mathbf{Q}_{\mu|\nu}^{(K)} := (Q_{\mu|\nu}^{(K)}(n))_{n \in [K]}$, we have*

$$\mathbb{E} \left[\left\| \mathbf{Q}_{\hat{\mu}_N|\nu}^{(K)} - \mathbf{Q}_{\mu|\nu}^{(K)} \right\|_1 \right] \leq \frac{K+1}{2\sqrt{N}}.$$

Proof. Fix $n \in [K]$ and define, for $x \in \mathbb{R}$,

$$\varphi_n(x) := \mathbb{P}_{\tilde{Y}_1, \dots, \tilde{Y}_K \sim \nu} \left(\#\{j \in [K] : \tilde{Y}_j \leq x\} = n \right). \quad (14)$$

Then, $0 \leq \varphi_n(x) \leq 1$ for all x . By Equation (10),

$$Q_{\mu|\nu}^{(K)}(n) = \mathbb{P}(A_{\mu|\nu}^{(K)} = n) = \mathbb{E}_{\mu}[\varphi_n] \text{ and } Q_{\hat{\mu}_N|\nu}^{(K)}(n) = \mathbb{E}_{\hat{\mu}_N}[\varphi_n] = \int_{\mathbb{R}} \varphi_n(x) d\hat{\mu}_N(x) = \frac{1}{N} \sum_{i=1}^N \varphi_n(X_i).$$

Thus, for each n ,

$$Q_{\hat{\mu}_N|\nu}^{(K)}(n) - Q_{\mu|\nu}^{(K)}(n) = \frac{1}{N} \sum_{i=1}^N (\varphi_n(X_i) - \mathbb{E}_{\mu}[\varphi_n]).$$

Since $X_1, \dots, X_N \stackrel{\text{i.i.d.}}{\sim} \mu$ and $\varphi_n: \mathbb{R} \rightarrow [0, 1]$ is a fixed deterministic function, the random variables $\varphi_n(X_1), \dots, \varphi_n(X_N)$ are also i.i.d. and take values in $[0, 1]$ with $\mathbb{V}(\varphi_n(X_1)) \leq \frac{1}{4}$. Set

$$Z_i := \varphi_n(X_i) - \mathbb{E}_{\mu}[\varphi_n], \quad i \in \{1, \dots, N\}.$$

Then $(Z_i)_{i=1}^N$ are i.i.d. and centered, so by independence

$$\mathbb{V}(Q_{\hat{\mu}_N|\nu}^{(K)}(n) - Q_{\mu|\nu}^{(K)}(n)) = \mathbb{V}\left(\frac{1}{N} \sum_{i=1}^N Z_i\right) = \frac{1}{N^2} \sum_{i=1}^N \mathbb{V}(Z_i) = \frac{1}{N} \mathbb{V}(Z_1) = \frac{1}{N} \mathbb{V}(\varphi_n(X_1)) \leq \frac{1}{4N}.$$

Applying Cauchy–Schwarz yields

$$\mathbb{E}\left[\left\|\mathbf{Q}_{\hat{\mu}_N|\nu}^{(K)} - \mathbf{Q}_{\mu|\nu}^{(K)}\right\|_1\right] \leq \sum_{n=0}^K \mathbb{E}[|Q_{\hat{\mu}_N|\nu}^{(K)}(n) - Q_{\mu|\nu}^{(K)}(n)|] \leq \sum_{n=0}^K \sqrt{\mathbb{V}(Q_{\hat{\mu}_N|\nu}^{(K)}(n) - Q_{\mu|\nu}^{(K)}(n))} \leq \frac{K+1}{2\sqrt{N}}.$$

□

Lemma B.5 (Sampling ν only). *Fix $K \in \mathbb{N}$. Let $\nu \in \mathcal{P}(\mathbb{R})$ and let $\hat{\nu}_M$ be the empirical measure based on M i.i.d. samples from ν . Then for any $\mu \in \mathcal{P}(\mathbb{R})$,*

$$\mathbb{E}\left[\left\|\mathbf{Q}_{\mu|\hat{\nu}_M}^{(K)} - \mathbf{Q}_{\mu|\nu}^{(K)}\right\|_1\right] \leq K \sqrt{\frac{2\pi}{M}},$$

where \mathbf{Q} is defined in Lemma B.4. In particular, the bound holds uniformly in μ .

Proof. Fix $\mu \in \mathcal{P}(\mathbb{R})$ and $K \in \mathbb{N}$. Let R_{ν} and $R_{\hat{\nu}_M}$ denote the CDFs of ν and $\hat{\nu}_M$. By (10),

$$Q_{\mu|\nu}^{(K)}(n) = \mathbb{E}_{\mu}[b_{n,K}(R_{\nu})], \quad Q_{\mu|\hat{\nu}_M}^{(K)}(n) = \mathbb{E}_{\mu}[b_{n,K}(R_{\hat{\nu}_M})].$$

By a simple coupling argument (alternatively combine [27, Eq. (3)] with [26, Eq. (4)]),

$$\sum_{n=0}^K |b_{n,K}(t) - b_{n,K}(s)| = 2 d_{\text{TV}}(\text{Bin}(K, s), \text{Bin}(K, t)) \leq K |s - t|.$$

Now fix a realization of $\hat{\nu}_M$. For any $x \in \mathbb{R}$ we have

$$\sum_{n=0}^K |b_{n,K}(R_{\hat{\nu}_M}(x)) - b_{n,K}(R_{\nu}(x))| \leq 2K |R_{\hat{\nu}_M}(x) - R_{\nu}(x)|.$$

Hence,

$$\begin{aligned} \|\mathbf{Q}_{\mu|\hat{\nu}_M} - \mathbf{Q}_{\mu|\nu}\|_1 &= \sum_{n=0}^K \left| \mathbb{E}_\mu [b_{n,K}(R_{\hat{\nu}_M})] - \mathbb{E}_\mu [b_{n,K}(R_\nu)] \right| \leq \mathbb{E}_\mu \left[\sum_{n=0}^K |b_{n,K}(R_{\hat{\nu}_M}) - b_{n,K}(R_\nu)| \right] \\ &\leq 2K \mathbb{E}_\mu [|R_{\hat{\nu}_M} - R_\nu|] \leq 2K \sup_{x \in \mathbb{R}} |R_{\hat{\nu}_M}(x) - R_\nu(x)|. \end{aligned}$$

Taking expectations over $\hat{\nu}_M$ and applying the Dvoretzky–Kiefer–Wolfowitz (DKW) inequality [34],

$$\mathbb{P}\left(\sup_{x \in \mathbb{R}} |R_{\hat{\nu}_M}(x) - R_\nu(x)| > t\right) \leq 2e^{-2Mt^2}, \quad t > 0,$$

we obtain

$$\mathbb{E}\left[\sup_{x \in \mathbb{R}} |R_{\hat{\nu}_M}(x) - R_\nu(x)|\right] = \int_0^\infty \mathbb{P}\left(\sup_{x \in \mathbb{R}} |R_{\hat{\nu}_M}(x) - R_\nu(x)| > t\right) dt \leq \int_0^\infty 2e^{-2Mt^2} dt = \sqrt{\frac{\pi}{2M}}.$$

Combining the two displays yields

$$\mathbb{E}\left[\|\mathbf{Q}_{\mu|\hat{\nu}_M} - \mathbf{Q}_{\mu|\nu}\|_1\right] \leq 2K \sqrt{\frac{\pi}{2M}}.$$

The bound is uniform in μ because μ does not appear on the right-hand side. \square

B.6 Proof of the univariate finite sample complexity bound Theorem 2.6

Theorem 2.6 (Univariate finite sample complexity). *Let $\mu, \nu \in \mathcal{P}(\mathbb{R})$ and $\hat{\mu}_N$ and $\hat{\nu}_M$ be their corresponding empirical measures with sample sizes N and M . For a fixed rank resolution K , if f is L_f -Lipschitz on $[0, K+1]$, then the expected estimation error satisfies*

$$\mathbb{E}\left[\left|D_{f,\hat{\nu}_M}^{(K)}(\hat{\mu}_N) - D_{f,\nu}^{(K)}(\mu)\right|\right] \leq L_f(K+1)\sqrt{2\pi} \left(\frac{1}{\sqrt{N}} + \frac{1}{\sqrt{M}}\right).$$

Proof of Theorem 2.6. For $K \in \mathbb{N}$ we have

$$\begin{aligned} \left|D_{f,\hat{\nu}_M}^{(K)}(\hat{\mu}_N) - D_{f,\nu}^{(K)}(\mu)\right| &\leq \frac{1}{K+1} \sum_{n=0}^K \left|f\left((K+1)Q_{\hat{\mu}_N|\hat{\nu}_M}^{(K)}(n)\right) - f\left((K+1)Q_{\mu|\nu}^{(K)}(n)\right)\right| \\ &\leq \frac{1}{K+1} \sum_{n=0}^K L_f(K+1) \left|Q_{\hat{\mu}_N|\hat{\nu}_M}^{(K)}(n) - Q_{\mu|\nu}^{(K)}(n)\right| \\ &= L_f \sum_{n=0}^K \left|Q_{\hat{\mu}_N|\hat{\nu}_M}^{(K)}(n) - Q_{\mu|\nu}^{(K)}(n)\right|, \end{aligned} \tag{15}$$

since for each $n \in [K]$, the quantities $(K+1)Q_{\hat{\mu}_N|\hat{\nu}_M}^{(K)}(n)$ and $(K+1)Q_{\mu|\nu}^{(K)}(n)$ lie in the interval $[0, K+1]$, and f is L_f -Lipschitz on $[0, K+1]$. Taking expectations, we obtain

$$\mathbb{E}\left[\left|D_f^{(K)}(\hat{\mu}_N \mid \hat{\nu}_M) - D_f^{(K)}(\mu \mid \nu)\right|\right] \leq L_f \mathbb{E}\left[\sum_{n=0}^K \left|Q_{\hat{\mu}_N|\hat{\nu}_M}^{(K)}(n) - Q_{\mu|\nu}^{(K)}(n)\right|\right]. \tag{16}$$

We now decompose the rank-pmf error into two contributions: the error due to sampling μ and the error due to sampling ν . By the triangle inequality,

$$\sum_{n=0}^K |Q_{\hat{\mu}_N|\hat{\nu}_M}^{(K)}(n) - Q_{\mu|\nu}^{(K)}(n)| \leq \sum_{n=0}^K |Q_{\hat{\mu}_N|\hat{\nu}_M}^{(K)}(n) - Q_{\hat{\mu}_N|\nu}^{(K)}(n)| + \sum_{n=0}^K |Q_{\hat{\mu}_N|\nu}^{(K)}(n) - Q_{\mu|\nu}^{(K)}(n)|.$$

Taking expectations and applying Lemma B.5 (which holds uniformly with respect to the argument of $D_{f,\nu}^{(K)}$, so it can be used with the random $\hat{\mu}_N$) and Lemma B.4, we obtain

$$\begin{aligned} \mathbb{E} \left[\sum_{n=0}^K |Q_{\hat{\mu}_N|\hat{\nu}_M}^{(K)}(n) - Q_{\mu|\nu}^{(K)}(n)| \right] &\leq \mathbb{E} \left[\sum_{n=0}^K |Q_{\hat{\mu}_N|\hat{\nu}_M}^{(K)}(n) - Q_{\hat{\mu}_N|\nu}^{(K)}(n)| \right] + \mathbb{E} \left[\sum_{n=0}^K |Q_{\hat{\mu}_N|\nu}^{(K)}(n) - Q_{\mu|\nu}^{(K)}(n)| \right] \\ &\leq 2K \sqrt{\frac{\pi}{2M}} + \frac{K+1}{2\sqrt{N}} \leq (K+1)\sqrt{2\pi} \left(\frac{1}{\sqrt{N}} + \frac{1}{\sqrt{M}} \right), \end{aligned} \tag{17}$$

where we used $\frac{1}{2} \leq \sqrt{2\pi}$ to simplify the constants. \square

B.7 Proof of the concentration bound

Proposition 2.7 (Concentration bound). *Let $K \in \mathbb{N}$ be fixed, and let $\hat{\mu}_N, \hat{\nu}_M$ be the empirical measures based on N and M i.i.d. samples from $\mu, \nu \in \mathcal{P}(\mathbb{R})$, respectively. If f is L_f -Lipschitz on $[0, K+1]$, then for any $\delta > 0$, with probability at least $1 - \delta$, we have*

$$|D_{f,\hat{\nu}_M}^{(K)}(\hat{\mu}_N) - \mathbb{E}[D_{f,\hat{\nu}_M}^{(K)}(\hat{\mu}_N)]| \leq L_f(K+1) \sqrt{2 \log(2/\delta) \left(\frac{1}{N} + \frac{1}{M} \right)}.$$

Proof. Let $K \in \mathbb{N}$ and define the functional

$$F(X_1, \dots, X_N, Y_1, \dots, Y_M) := D_{f,\hat{\nu}_M}^{(K)}(\hat{\mu}_N),$$

where the empirical measures $\hat{\mu}_N$ and $\hat{\nu}_M$ are given by (4). We will apply *McDiarmid's bounded differences inequality* (see [8, Sec 6]) to F . We first quantify how much F can change when we replace one observation X_i in the sample from μ , while keeping all other data points fixed. Consider two datasets that differ only in the i -th sample from μ :

$$(X_1, \dots, X_i, \dots, X_N, Y_1, \dots, Y_M), \quad (X_1, \dots, X'_i, \dots, X_N, Y_1, \dots, Y_M),$$

and fix Y_1, \dots, Y_M . Thus $\hat{\nu}_M$ is the same in both cases, while the empirical measure of μ changes from $\hat{\mu}_N$ to

$$\hat{\mu}'_N = \hat{\mu}_N - \frac{1}{N} \delta_{X_i} + \frac{1}{N} \delta_{X'_i}.$$

Fix $\hat{\nu}_M$ and $K \in \mathbb{N}$. For each $n \in [K]$ define φ_n by (14). Again,

$$Q_{\hat{\mu}_N|\hat{\nu}_M}^{(K)}(n) = \frac{1}{N} \sum_{k=1}^N \varphi_n(X_k), \quad Q_{\hat{\mu}'_N|\hat{\nu}_M}^{(K)}(n) = \frac{1}{N} \sum_{k=1}^N \varphi_n(X'_k),$$

where $X'_k = X_k$ for $k \neq i$ and $X'_i = X'_i$. Hence

$$Q_{\hat{\mu}'_N | \hat{\nu}_M}^{(K)}(n) - Q_{\hat{\mu}_N | \hat{\nu}_M}^{(K)}(n) = \frac{1}{N} (\varphi_n(X'_i) - \varphi_n(X_i)).$$

Since $0 \leq \varphi_n \leq 1$, we obtain

$$\|Q_{\hat{\mu}'_N | \hat{\nu}_M}^{(K)} - Q_{\hat{\mu}_N | \hat{\nu}_M}^{(K)}\|_1 \leq \frac{K+1}{N}.$$

Applying Equation (15) with $(\hat{\mu}'_N | \hat{\nu}_M)$ instead of $(\mu | \nu)$, we obtain

$$\begin{aligned} & |F(X_1, \dots, X'_i, \dots, X_N, Y_1, \dots, Y_M) - F(X_1, \dots, X_i, \dots, X_N, Y_1, \dots, Y_M)| \\ &= |D_{f, \hat{\nu}_M}^{(K)}(\hat{\mu}'_N) - D_{f, \hat{\nu}_M}^{(K)}(\hat{\mu}_N)| \leq L_f \|Q_{\hat{\mu}'_N | \hat{\nu}_M}^{(K)} - Q_{\hat{\mu}_N | \hat{\nu}_M}^{(K)}\|_1 \leq L_f \frac{K+1}{N}. \end{aligned}$$

Now, consider two datasets that differ only in Y_j :

$$(X_1, \dots, X_N, Y_1, \dots, Y_j, \dots, Y_M), \quad (X_1, \dots, X_N, Y_1, \dots, Y'_j, \dots, Y_M),$$

so that $\hat{\mu}_N$ is fixed, while the empirical measure of ν changes from $\hat{\nu}_M$ to $\hat{\nu}'_M = \hat{\nu}_M - \frac{1}{M} \delta_{Y_j} + \frac{1}{M} \delta_{Y'_j}$. Changing a single atom in an empirical measure of size M changes the CDF by at most $1/M$, that is,

$$\sup_{x \in \mathbb{R}} |R_{\hat{\nu}'_M}(x) - R_{\hat{\nu}_M}(x)| \leq \frac{1}{M}.$$

As in the proof of Lemma B.5, we obtain

$$\begin{aligned} & \|Q_{\hat{\mu}_N | \hat{\nu}'_M}^{(K)} - Q_{\hat{\mu}_N | \hat{\nu}_M}^{(K)}\|_1 = \sum_{n=0}^K \left| \mathbb{E}_{\hat{\mu}_N} [b_{n,K}(R_{\hat{\nu}'_M})] - \mathbb{E}_{\hat{\mu}_N} [b_{n,K}(R_{\hat{\nu}_M})] \right| \\ & \leq \mathbb{E}_{\hat{\mu}_N} \left[\sum_{n=0}^K |b_{n,K}(R_{\hat{\nu}'_M}) - b_{n,K}(R_{\hat{\nu}_M})| \right] \\ & \leq 2K \mathbb{E}_{\hat{\mu}_N} [|R_{\hat{\nu}'_M} - R_{\hat{\nu}_M}|] \leq 2K \sup_{x \in \mathbb{R}} |R_{\hat{\nu}'_M}(x) - R_{\hat{\nu}_M}(x)| \leq \frac{2K}{M}. \end{aligned}$$

Applying Equation (15) with and $(\hat{\mu}_N, \hat{\nu}'_M)$ instead of $(\mu | \nu)$, we obtain

$$\begin{aligned} & |F(X_1, \dots, X_N, Y_1, \dots, Y'_j, \dots, Y_M) - F(X_1, \dots, X_N, Y_1, \dots, Y_j, \dots, Y_M)| \\ &= |D_{f, \hat{\nu}'_M}^{(K)}(\hat{\mu}_N) - D_{f, \hat{\nu}_M}^{(K)}(\hat{\mu}_N)| \leq L_f \|Q_{\hat{\mu}_N | \hat{\nu}'_M}^{(K)} - Q_{\hat{\mu}_N | \hat{\nu}_M}^{(K)}\|_1 \leq L_f \frac{2K}{M}. \end{aligned}$$

We have shown that F satisfies the bounded differences condition with

$$c_i = L_f \frac{K+1}{N} \quad (i = 1, \dots, N), \quad c_{N+j} = L_f \frac{2K}{M} \quad (j = 1, \dots, M).$$

Hence, using $K^2 \leq (K+1)^2$,

$$\sum_{i=1}^{N+M} c_i^2 = \sum_{i=1}^N \left(L_f \frac{K+1}{N} \right)^2 + \sum_{j=1}^M \left(L_f \frac{2K}{M} \right)^2 \leq 4L_f^2 (K+1)^2 \left(\frac{1}{N} + \frac{1}{M} \right),$$

By McDiarmid's inequality (Theorem 6.2 in [8]), for any $t > 0$,

$$\mathbb{P}\left(|F - \mathbb{E}[F]| \geq t\right) \leq 2 \exp\left(-\frac{2t^2}{\sum_{i=1}^{N+M} c_i^2}\right) \leq 2 \exp\left(-\frac{t^2}{2L_f^2(K+1)^2\left(\frac{1}{N} + \frac{1}{M}\right)}\right).$$

Let $\delta > 0$ and choose

$$t = L_f(K+1)\sqrt{2\log(2/\delta)\left(\frac{1}{N} + \frac{1}{M}\right)}.$$

Then

$$\mathbb{P}\left(|F - \mathbb{E}[F]| \geq t\right) \leq \delta.$$

Since $F = D_{f,\hat{\nu}_M}^{(K)}(\hat{\mu}_N)$, this is exactly the desired bound: with probability at least $1 - \delta$,

$$|D_{f,\hat{\nu}_M}^{(K)}(\hat{\mu}_N) - \mathbb{E}[D_{f,\hat{\nu}_M}^{(K)}(\hat{\mu}_N)]| \leq L_f(K+1)\sqrt{\frac{\log(2/\delta)}{2}\left(\frac{1}{N} + \frac{1}{M}\right)}. \quad \square$$

B.8 Proof of the asymptotic normality Theorem 3.3

Theorem 3.3 (Asymptotic normality, sliced one-sample case). *Fix $K \in \mathbb{N}$ and $\mu, \nu \in \mathcal{P}(\mathbb{R}^d)$ with $\mu \neq \nu$ and $D_{f,\nu}^{(K)}(\mu) > 0$, and form the empirical approximation $\hat{\mu}_N$ from (4). If $f \in \mathcal{C}^1([0, K+1])$, then there exists a constant $\tau_K^2 > 0$ such that, in distribution,*

$$\sqrt{N}\left(D_{f,\nu}^{(K)}(\hat{\mu}_N) - D_{f,\nu}^{(K)}(\mu)\right) \xrightarrow[N \rightarrow \infty]{d} \mathcal{N}(0, \tau_K^2).$$

Proof. 1. For each direction $s \in \mathbb{S}^{d-1}$ and $n \in [K]$, define $\varphi_{n,s} : \mathbb{R}^d \rightarrow [0, 1]$ as the probability that a sample x has rank n among K draws $\tilde{Y}_1, \dots, \tilde{Y}_K \stackrel{\text{i.i.d.}}{\sim} \nu$ when both are projected along s , i.e.,

$$\varphi_{n,s}(x) := \mathbb{P}\left(\#\{j \in [K] : s^\top \tilde{Y}_j \leq s^\top x\} = n\right).$$

As in the univariate case (compare (10)) one checks that for any $\mu \in \mathcal{P}(\mathbb{R}^d)$ and $s \in \mathbb{S}^{d-1}$,

$$Q_{\mu_s|\nu_s}^{(K)}(n) = \mathbb{E}_\mu[\varphi_{n,s}] \quad \text{and} \quad Q_{(\hat{\mu}_N)_s|\nu_s}^{(K)}(n) = \frac{1}{N} \sum_{i=1}^N \varphi_{n,s}(X_i), \quad (18)$$

where the empirical version $\hat{\mu}_N$ is defined in (4). Define the Hilbert space $\mathcal{H} := L^2(\mathbb{S}^{d-1} \times [K], \sigma \otimes U_K)$ with inner product

$$\langle h, g \rangle_{\mathcal{H}} := \int_{\mathbb{S}^{d-1}} \frac{1}{K+1} \sum_{n=0}^K h(s, n) g(s, n) d\sigma(s), \quad g, h \in \mathcal{H}.$$

For $x \in \mathbb{R}^d$, define the random element $\Phi(x) \in \mathcal{H}$ by $\Phi(x)(s, n) := \varphi_{n,s}(x)$. Then $\|\Phi(x)\|_{\mathcal{H}} \leq 1$ because $0 \leq \varphi_{n,s}(x) \leq 1$. Let

$$T := \mathbb{E}_\mu[\Phi] \in \mathcal{H}, \quad T_N := \frac{1}{N} \sum_{i=1}^N \Phi(X_i) \in \mathcal{H}.$$

By the identities (18), we have

$$T(s, n) = \mathbb{E}_\mu[\varphi_{n, s}] = Q_{\mu_s | \nu_s}^{(K)}(n), \quad T_N(s, n) = Q_{(\hat{\mu}_N)_s | \nu_s}^{(K)}(n).$$

The random elements $(\Phi(X_k))_{k \in \mathbb{N}}$ are i.i.d. in \mathcal{H} with $\mathbb{E}_\mu[\|\Phi\|_{\mathcal{H}}^2] \leq 1$. Hence the standard central limit theorem in separable Hilbert spaces applies, and we obtain

$$\sqrt{N}(T_N - T) \xrightarrow{d} \mathcal{G} \quad \text{in } \mathcal{H},$$

where \mathcal{G} is a mean-zero Gaussian element in \mathcal{H} with covariance operator determined by Φ .

2. We now write the rank-statistic f -divergence and its approximation by samples as $\Psi(T)$ and $\Psi(T_N)$ for some Ψ and use the delta-method.

Indeed, for

$$\Psi: \mathcal{H} \rightarrow \mathbb{R}, \quad h \mapsto \int_{\mathbb{S}^{d-1}} \frac{1}{K+1} \sum_{n=0}^K f((K+1)h(s, n)) d\sigma(s)$$

we have

$$D_{f, \nu}^{(K)}(\mu) = \Psi(T) = \int_{\mathbb{S}^{d-1}} \frac{1}{K+1} \sum_{n=0}^K f((K+1)Q_{\mu | \nu_s}^{(K)}(n)) d\sigma(s) \quad \text{and} \quad D_{f, \nu}^{(K)}(\hat{\mu}_N) = \Psi(T_N).$$

We now show that Ψ is differentiable. Since $f \in C^1([0, K+1])$, Ψ is Fréchet differentiable at T , with derivative

$$D\Psi(T): \mathcal{H} \rightarrow \mathbb{R}, \quad h \mapsto \int_{\mathbb{S}^{d-1}} \sum_{n=0}^K f'((K+1)T(s, n)) h(s, n) d\sigma(s).$$

In particular, at $T(s, n) = Q_{\mu_s | \nu_s}^{(K)}(n)$ this becomes

$$D\Psi(T)[h] = \int_{\mathbb{S}^{d-1}} \sum_{n=0}^K f'((K+1)Q_{\mu_s | \nu_s}^{(K)}(n)) h(s, n) d\sigma(s),$$

which defines a bounded linear functional on \mathcal{H} .

By the Hilbert-space delta method [53, Thm. 3.9.4], the combination of the CLT for T_N and the Fréchet differentiability of Ψ at T implies

$$\sqrt{N}(\Psi(T_N) - \Psi(T)) \xrightarrow{d} \mathcal{N}(0, \tau_K^2),$$

with asymptotic variance

$$\tau_K^2 = \mathbb{V}(D\Psi(T)[\Phi(X_1) - T]) > 0,$$

where the positivity follows from the non-degeneracy assumption $D_{f, \sigma}^{(K)}(\mu | \nu) > 0$ together with mild regularity (for instance, whenever the linear functional $h \mapsto D\Psi(T)[h]$ is not almost surely constant on the support of $\Phi(X_1)$).

Recalling that $\Psi(T) = D_{f, \nu}^{(K)}(\mu)$ and $\Psi(T_N) = D_{f, \nu}^{(K)}(\hat{\mu}_N)$, we obtain the desired conclusion. \square

C Experiments

C.1 Neural vs. rank-statistic divergence estimation across dimensions

This appendix provides the full experimental details for the benchmark in Section 4 comparing the proposed rank-statistic estimator to the neural KL-divergence estimator of [51] on the truncated-Gaussian vs. uniform setup.

Distributions and supports. For each dimension $d \in \{2, 5, 10\}$, the target distribution μ is the standard Gaussian $\mathcal{N}(0, I_d)$ truncated (and renormalized) to an axis-aligned box X , and the reference distribution is the uniform measure $\nu = \text{Unif}(X)$. Concretely,

$$X_2 = [0.1, 2] \times [-1, 0], \quad X_5 = [0.1, 2] \times [-1, 0] \times [2, 3] \times [-2, -1.5] \times [-1, 1],$$

and for $d = 10$ we use the product support $X_{10} = X_5 \times X_5$. Sampling from ν is done by drawing each coordinate independently and uniformly over the corresponding interval. Sampling from μ is done by accept–reject: draw from $\mathcal{N}(0, I_d)$ until the sample falls in X .

Sample sizes and repetitions. For each n in $n \in 10^4 \cdot \{1, 2, 4, 8, 16, 32, 64, 128, 256, 512\}$ we draw n i.i.d. samples from μ and n i.i.d. samples from ν , and repeat the whole procedure over $R = 10$ independent random seeds. Figure 2 reports the mean and ± 1 standard deviation bands over these runs (for both estimators).

Analytic KL reference. In this benchmark, the “ground-truth” $\text{KL}(\mu\|\nu)$ shown as a dashed line in Figure 2 is computed analytically (no additional Monte Carlo layer). Let $\tilde{\mu} = \mathcal{N}(0, I_d)$ denote the untruncated Gaussian density and let $X = \prod_{j=1}^d [a_j, b_j]$ be the truncation box. The truncated density is $p_\mu(x) = \tilde{p}(x) \mathbf{1}\{x \in X\}/Z$, where $Z = \int_X \tilde{p}(x) dx$ is the truncation mass, and $p_\nu(x) = 1/\text{Vol}(X)$ for $x \in X$. Using $\text{KL}(\mu\|\nu) = \mathbb{E}_\mu[\log p_\mu(X) - \log p_\nu(X)]$ and separability of the standard Gaussian, Z factorizes as $Z = \prod_{j=1}^d (\Phi(b_j) - \Phi(a_j))$, where Φ denotes the CDF of the standard normal distribution (and φ its density). The remaining expectation reduces to the sum of one-dimensional truncated moments $\mathbb{E}_\mu[X_j^2]$ (available in closed form via φ and Φ). This yields an exact value for each d and box X ; the implementation follows these standard identities.

Neural baseline (full protocol). We compare against the neural KL-divergence estimator of [51] and follow their protocol exactly. For each sample size n , the network width is set to $k = \lceil n^{1/5} \rceil$ and the model is trained for 200 epochs with Adam, using learning rate 10^{-2} and a single decay to 10^{-3} after 100 epochs. Minibatches have size $10^{-3}n$. Results are averaged over the same $R = 10$ seeds used for the rank-based estimator. (All remaining hyperparameters and architectural details are as in [51].)

Rank-statistic estimator settings. In contrast, the rank-statistic estimator requires no iterative optimization: once the samples are fixed, the estimate is fully determined by the rank resolution K and (in the multivariate construction) the number of random projections L . In this benchmark, the sliced KL estimate is computed by averaging the 1D rank-statistic KL over L random directions (sampled uniformly on the sphere) and, when reporting a multivariate proxy, rescaling by d as in

the main text. Unless stated otherwise, all randomness in the rank estimator comes solely from (i) the sampled data and (ii) the sampled directions.

C.2 Univariate empirical convergence and the influence of resolution K

This appendix provides additional implementation details for the one-dimensional benchmarks reported in Section 4.2. For each configuration we draw n_μ i.i.d. samples from μ and n_ν i.i.d. samples from ν , construct the Bernstein rank histogram $Q_{\mu|\nu}^{(K)}$, and compute the corresponding discrete f -divergence $D_{f,\nu}^{(K)}(\mu)$. We repeat each setting for $R = 10$ seeds and report mean±std.

Distributions and supports. We study four representative mismatch families that collectively capture shifts in location and scale, departures from unimodality, and tail mismatch:

- Location shift (Gaussian mean). We set $\mu = \mathcal{N}(0, 1)$ and $\nu = \mathcal{N}(\Delta, 1)$ with $\Delta \in \{0, 0.5, 1, 2\}$, and report JS , KL , and TV .
- Scale change (Gaussian variance). We take $\mu = \mathcal{N}(0, 1)$ and $\nu = \mathcal{N}(0, \sigma)$ for $\sigma \in \{1, 1.2, 1.5, 2\}$, and report KL , squared Hellinger ($Hell^2$), and TV .
- Multimodality (mixture vs. unimodal). To probe sensitivity to multiple modes, we compare the symmetric mixture $\mu = \frac{1}{2}\mathcal{N}(-\Delta, 1) + \frac{1}{2}\mathcal{N}(+\Delta, 1)$ against $\nu = \mathcal{N}(0, 1)$ over the same Δ values, and report JS , KL , and TV .
- Tail mismatch (heavy-tailed vs. Gaussian). Finally, we compare $\mu = \text{Laplace}(0, 1)$ to $\nu = \mathcal{N}(0, 1)$ and report JS , KL , and TV .

Unless stated otherwise we use $n_\mu = n_\nu = 10,000$, and we evaluate $K \in \{32, 64, 128, 256, 512\}$.

Reference Whenever a closed form is available, we use it as ground truth (in particular, Gaussian–Gaussian KL, squared Hellinger, and TV for Gaussian mean/scale changes). For Jensen–Shannon (JS), we compute a high-accuracy reference from

$$JS(\mu, \nu) = \frac{1}{2} \mathbb{E}_{X \sim \mu} \left[\log \frac{2p_\mu(X)}{p_\mu(X) + p_\nu(X)} \right] + \frac{1}{2} \mathbb{E}_{Y \sim \nu} \left[\log \frac{2p_\nu(Y)}{p_\mu(Y) + p_\nu(Y)} \right],$$

and evaluate the resulting one-dimensional expectations by numerical quadrature with a tight tolerance. All evaluations are carried out in the log domain to avoid numerical issues in the tails. In the mixture–vs–Gaussian setting, the mixture density p_μ is computed exactly as the average of its two Gaussian components inside the same procedure.

For settings where our reference is not available in closed form in our implementation, namely, mixture–vs–Gaussian KL and TV, as well as $\text{Laplace}(0, 1)$ vs. $\mathcal{N}(0, 1)$ for JS/KL/TV, we compute a single high-sample Monte Carlo reference once and reuse it across all R runs. Specifically, we draw $n_{\text{ref}} = 10^7$ i.i.d. samples from each distribution and plug them into the corresponding expectation identity (JS as above, and analogously for KL/TV).

For each configuration and each K , we report the estimate $\hat{D}_{f,\nu}^{(K)}(\mu)$ (mean±std over R seeds) and the ratio $\hat{D}_{f,\nu}^{(K)}(\mu)/D_{f,\nu}(\mu)$ to summarize the finite- K approximation gap.

Results Taken together, Table 2 and Figures 7–9 show that increasing the rank resolution K systematically closes the finite- K gap: the estimate/reference ratio moves toward 1 across all mismatch families and all reported divergences (JS, KL, Hell², and the added TV), with near-unbiased behaviour already for moderate K in the smooth Gaussian cases (mean/scale shifts), while multimodality and tail mismatch require larger K to reduce bias and typically exhibit larger finite-sample variability. In particular, TV is already accurate at moderate K in the Gaussian settings (after the $\frac{1}{2}$ conversion from the ℓ_1 form returned by our implementation), whereas KL under heavy tails remains substantially underestimated even at the largest K considered, reflecting the increased difficulty of capturing tail contributions with finite rank resolution. At fixed $K = 256$, the estimator remains stable across a range of shift magnitudes and scales, as summarized in Figure 8. The K -sweeps in Figure 7 and, especially, the log–log plot in Figure 9 further clarify the convergence hierarchy by visualizing the absolute ratio error $|1 - \text{Ratio}|$ versus K : the Gaussian scale-change case decays the fastest (tracking a near-optimal $\mathcal{O}(K^{-1})$ slope), the Gaussian mean-shift case converges more slowly (consistent with reduced tail regularity), and the Laplace–vs–Gaussian heavy-tail mismatch improves the slowest, remaining closest to the shallowest guide slope. This separation matches the qualitative ordering suggested by the regularity-based rate discussion in the main text and motivates the larger- K settings used for the tail-mismatch experiments.

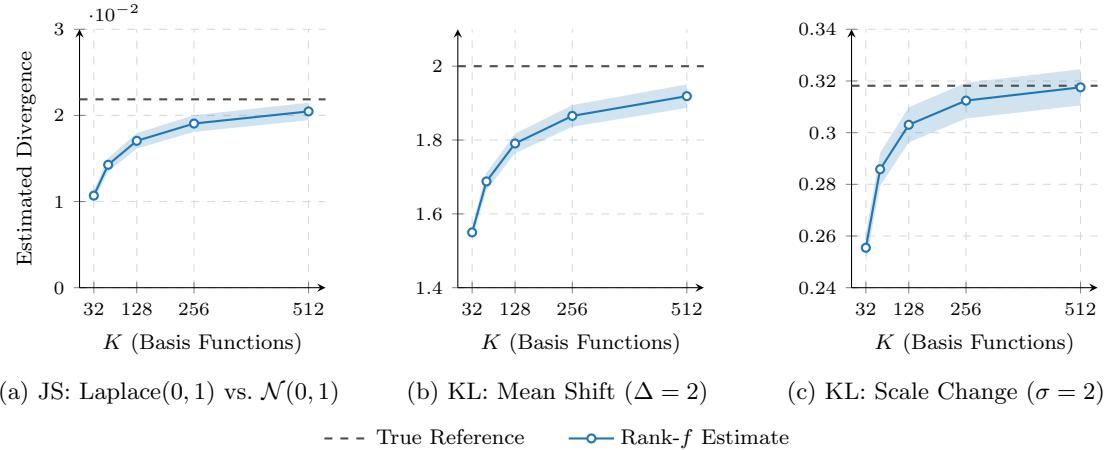


Figure 7: Convergence of the Rank- f estimator as the number of basis functions K increases. The estimator (blue) consistently converges to the true analytic or Monte Carlo reference (dashed gray) across different divergence types and scenarios.

C.3 Sliced rank-Statistic f -divergences: empirical convergence

This appendix provides the full experimental protocol underlying Section 4.3. For each configuration (dimension d and distribution pair (μ, ν)), we draw n_μ i.i.d. samples from μ and n_ν i.i.d. samples from ν , compute the sliced rank- f estimate using L random directions and rank order K , and repeat the procedure for R independent runs, reporting mean \pm std. Unless stated otherwise we use $K = 64$, $L = 128$, $n_\mu = n_\nu = 10,000$, and $R = 10$. Random directions are sampled uniformly on \mathbb{S}^{d-1} .

Family	Scen.	Param.	Ratio $D_{f,\nu}^{(K)}(\mu)$ for $K =$				
			32	64	128	256	512
Mean shift	JS	$\Delta = 0.5$	0.933 ± 0.040	0.968 ± 0.041	0.989 ± 0.042	1.003 ± 0.042	1.013 ± 0.042
		$\Delta = 1.0$	0.928 ± 0.033	0.961 ± 0.034	0.981 ± 0.035	0.992 ± 0.035	0.999 ± 0.035
		$\Delta = 2.0$	0.930 ± 0.008	0.962 ± 0.008	0.981 ± 0.009	0.991 ± 0.009	0.997 ± 0.009
	KL	$\Delta = 0.5$	0.946 ± 0.060	0.987 ± 0.063	1.013 ± 0.065	1.030 ± 0.066	1.044 ± 0.068
		$\Delta = 1.0$	0.880 ± 0.024	0.924 ± 0.025	0.952 ± 0.026	0.969 ± 0.027	0.980 ± 0.027
		$\Delta = 2.0$	0.775 ± 0.010	0.844 ± 0.012	0.895 ± 0.013	0.933 ± 0.015	0.959 ± 0.016
	TV	$\Delta = 0.5$	0.979 ± 0.026	0.991 ± 0.027	0.998 ± 0.027	1.001 ± 0.027	1.003 ± 0.027
		$\Delta = 1.0$	0.974 ± 0.011	0.985 ± 0.011	0.991 ± 0.011	0.994 ± 0.011	0.996 ± 0.011
		$\Delta = 2.0$	0.977 ± 0.002	0.989 ± 0.002	0.996 ± 0.002	0.999 ± 0.003	1.001 ± 0.003
Scale change	KL	$\sigma = 1.2$	0.743 ± 0.063	0.841 ± 0.070	0.908 ± 0.072	0.954 ± 0.072	0.991 ± 0.072
		$\sigma = 1.5$	0.779 ± 0.027	0.872 ± 0.029	0.927 ± 0.030	0.958 ± 0.031	0.977 ± 0.031
		$\sigma = 2.0$	0.803 ± 0.018	0.898 ± 0.020	0.953 ± 0.021	0.982 ± 0.022	0.998 ± 0.022
	Hell ²	$\sigma = 1.2$	0.741 ± 0.077	0.853 ± 0.089	0.931 ± 0.098	0.986 ± 0.106	1.029 ± 0.111
		$\sigma = 1.5$	0.735 ± 0.035	0.842 ± 0.039	0.908 ± 0.041	0.948 ± 0.042	0.973 ± 0.042
		$\sigma = 2.0$	0.744 ± 0.014	0.858 ± 0.014	0.926 ± 0.014	0.965 ± 0.013	0.987 ± 0.012
	TV	$\sigma = 1.2$	0.934 ± 0.033	0.970 ± 0.036	0.990 ± 0.039	1.001 ± 0.040	1.008 ± 0.041
		$\sigma = 1.5$	0.907 ± 0.014	0.948 ± 0.015	0.970 ± 0.017	0.982 ± 0.018	0.989 ± 0.018
		$\sigma = 2.0$	0.898 ± 0.009	0.947 ± 0.010	0.974 ± 0.010	0.988 ± 0.010	0.995 ± 0.010
Multimodal	JS	$\Delta = 0.5$	0.746 ± 0.157	0.849 ± 0.176	0.926 ± 0.189	0.994 ± 0.196	1.068 ± 0.199
		$\Delta = 1.0$	0.769 ± 0.038	0.849 ± 0.040	0.898 ± 0.041	0.929 ± 0.041	0.948 ± 0.042
		$\Delta = 2.0$	0.846 ± 0.019	0.912 ± 0.020	0.950 ± 0.021	0.972 ± 0.021	0.985 ± 0.021
	KL	$\Delta = 0.5$	0.742 ± 0.125	0.853 ± 0.147	0.936 ± 0.165	1.000 ± 0.178	1.054 ± 0.187
		$\Delta = 1.0$	0.766 ± 0.032	0.864 ± 0.036	0.930 ± 0.039	0.971 ± 0.041	0.998 ± 0.041
		$\Delta = 2.0$	0.669 ± 0.009	0.765 ± 0.010	0.837 ± 0.012	0.889 ± 0.013	0.926 ± 0.013
	TV	$\Delta = 0.5$	0.935 ± 0.066	0.969 ± 0.070	0.990 ± 0.074	1.005 ± 0.076	1.017 ± 0.078
		$\Delta = 1.0$	0.947 ± 0.023	0.975 ± 0.023	0.990 ± 0.023	0.998 ± 0.023	1.003 ± 0.024
		$\Delta = 2.0$	0.942 ± 0.005	0.969 ± 0.005	0.982 ± 0.005	0.989 ± 0.006	0.993 ± 0.006
Heavy tails	JS	–	0.488 ± 0.028	0.651 ± 0.036	0.778 ± 0.041	0.869 ± 0.044	0.933 ± 0.046
	KL	–	0.210 ± 0.012	0.299 ± 0.017	0.383 ± 0.022	0.458 ± 0.025	0.524 ± 0.028
	TV	–	0.824 ± 0.014	0.907 ± 0.017	0.955 ± 0.020	0.981 ± 0.023	0.996 ± 0.025

Table 2: 1D divergence estimation benchmarks (10 runs). We report the ratio estimate/reference (mean \pm std) for various K values.

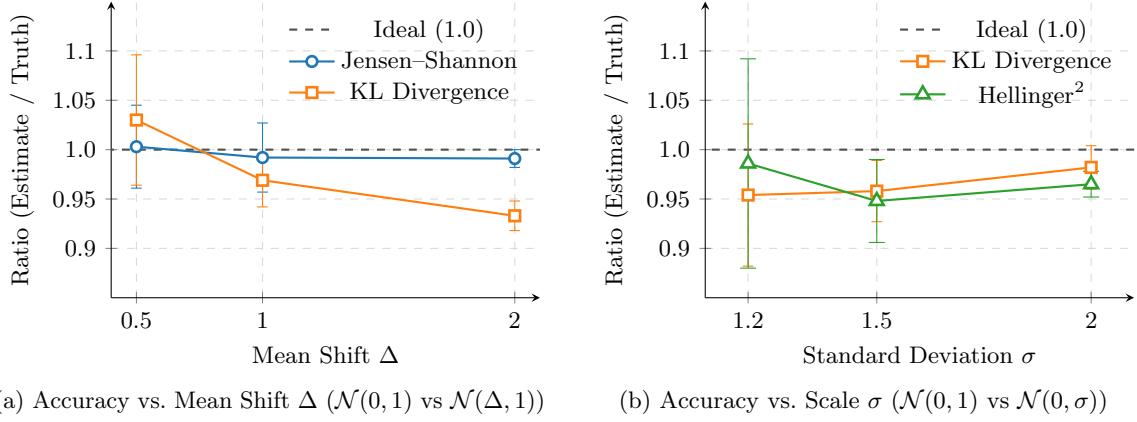


Figure 8: Robustness of the Rank- f estimator at fixed $K = 256$. The plots show the ratio of the estimated divergence to the ground truth (closer to 1.0 is better) as the shift (Δ) or scale (σ) increases.

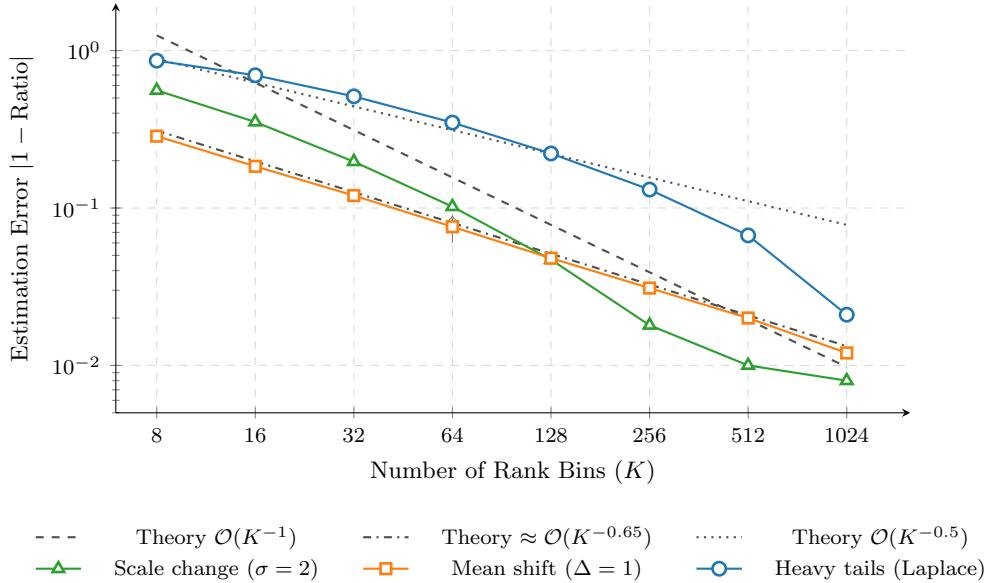


Figure 9: Convergence rate analysis across different tail behaviors. We compare the empirical error against theoretical slopes. The Scale Change (Green) is bounded and achieves the optimal $\mathcal{O}(K^{-1})$ rate. The Mean Shift (Orange) suffers from an unbounded density ratio at the tail, degrading convergence to $\approx \mathcal{O}(K^{-0.65})$. The Heavy Tail (Blue) case is the most difficult, bounded by the Hölder continuity limit of $\mathcal{O}(K^{-0.5})$.

Distribution families. We consider the following multivariate mismatch families (in dimension d): (i) Gaussian mean shifts, $\mu = \mathcal{N}(0, I_d)$ and $\nu = \mathcal{N}(\Delta e_1, I_d)$ with $\Delta \in \{0, 0.5, 1.0\}$; (ii) Gaussian scale changes, $\mu = \mathcal{N}(0, I_d)$ and $\nu = \mathcal{N}(0, \sigma^2 I_d)$ with $\sigma \in \{1.0, 1.2, 1.5, 2.0\}$; (iii) anisotropic Gaussian covariance mismatch, $\mu = \mathcal{N}(0, I_d)$ and $\nu = \mathcal{N}(0, \text{diag}(1, \dots, 2))$; and (iv) non-Gaussian comparisons, including factorized Laplace vs. Gaussian for JS, Student- t vs. Gaussian for KL, and a symmetric two-component Gaussian mixture vs. Gaussian for JS.

Scaling and reported ratios. Alongside the sliced estimate $D_{f,\nu}^{(K)}(\mu)$, we also report the simple normalization $d \times D_{f,\nu}^{(K)}(\mu)$ and summarize accuracy via the ratio $(d \times \text{sliced})/\text{true}$. This scaling is not intended to be exact in general; it is a lightweight calibration that keeps ratios on a comparable scale across dimensions.

Reference (“ground-truth”) divergences. Reference divergences are computed as follows, depending on whether closed forms are available:

- **Gaussian–Gaussian (analytic references).** For $\mu = \mathcal{N}(\mu_0, \Sigma_0)$ and $\nu = \mathcal{N}(\mu_1, \Sigma_1)$, the reference $\text{KL}(\mu\|\nu)$ and squared Hellinger $H^2(\mu, \nu)$ are evaluated in closed form. This avoids an additional numerical approximation layer, so discrepancies can be attributed to the rank-statistic estimator rather than to the reference computation.
- **Gaussian Jensen–Shannon (deterministic proxy).** The multivariate Jensen–Shannon divergence between two Gaussians does not admit a simple closed form because the mixture $\frac{1}{2}\mu + \frac{1}{2}\nu$ is not Gaussian. To keep the reference deterministic (and avoid injecting extra Monte Carlo variance), we approximate the mixture by a single Gaussian with matched mean and covariance (moment matching), and define the reference as $\frac{1}{2}\text{KL}(\mu\|M) + \frac{1}{2}\text{KL}(\nu\|M)$ for that matched Gaussian M .
- **Non-Gaussian pairs (Monte Carlo from known log-densities).** When at least one distribution is non-Gaussian (e.g., Laplace vs. Gaussian, Student- t vs. Gaussian, or a Gaussian mixture vs. Gaussian), a closed-form multivariate reference is typically unavailable. In these cases, the reference divergence is computed by Monte Carlo from its expectation form using the *known* log-densities (e.g., $\text{KL}(\mu\|\nu) = \mathbb{E}_\mu[\log p_\mu(X) - \log p_\nu(X)]$, and similarly for JS via expectations under μ and ν). All evaluations are performed in the log domain using log-sum-exp to ensure numerical stability.

Figure 3 and Table 3 provide complementary views of the same phenomenon. Figure 3 isolates the Gaussian mean-shift setting and shows that the normalized quantity $(d \times \text{sliced})/\text{true}$ remains close to the ideal value 1 across dimensions, with moderate, dimension-dependent deviations that are consistent with a mismatch between the sliced functional and the full multivariate divergence (and with the crudeness of the $d \times (\cdot)$ calibration). Table 3 summarizes this behavior across a broader set of distribution pairs: for Gaussian–Gaussian benchmarks (KL and Hellinger²) the ratios typically stay near 1, while JS experiments that rely on the Gaussian-proxy reference and non-Gaussian misspecification cases exhibit larger and more variable departures, especially as d grows, highlighting that the sliced estimator is best interpreted as a stable, sample-based surrogate whose absolute scale can drift from the multivariate reference in challenging regimes. Finally, Figure 10 illustrates how increasing the rank resolution K systematically reduces the finite- K approximation gap in representative cases, with ratios approaching the ideal baseline as K increases.

Setting	f -divergence	Parameter	Dimension d				
			2	5	10	20	50
Mean Shift	KL	$\Delta = 0.5$	1.015 ± 0.067	1.098 ± 0.052	1.188 ± 0.072	0.977 ± 0.060	1.304 ± 0.044
	KL	$\Delta = 1.0$	0.991 ± 0.030	1.087 ± 0.032	1.170 ± 0.031	0.899 ± 0.028	1.113 ± 0.042
	Hellinger ²	$\Delta = 0.5$	1.005 ± 0.062	0.935 ± 0.048	0.973 ± 0.049	1.002 ± 0.037	1.035 ± 0.060
	Hellinger ²	$\Delta = 1.0$	0.972 ± 0.033	0.931 ± 0.022	0.965 ± 0.048	0.943 ± 0.042	0.851 ± 0.021
	JS (Gaussian)	$\Delta = 0.5$	1.007 ± 0.076	0.899 ± 0.040	0.887 ± 0.031	1.006 ± 0.060	1.234 ± 0.038
	JS (Gaussian)	$\Delta = 1.0$	0.979 ± 0.043	0.892 ± 0.013	0.895 ± 0.035	0.951 ± 0.041	1.144 ± 0.031
Scale and Covariance	JS (Scale)	$\sigma = 1.2$	0.891 ± 0.052	0.936 ± 0.048	0.913 ± 0.030	0.851 ± 0.016	0.846 ± 0.016
	JS (Scale)	$\sigma = 1.5$	0.856 ± 0.027	0.856 ± 0.015	0.858 ± 0.013	0.797 ± 0.007	0.803 ± 0.006
	JS (Scale)	$\sigma = 2.0$	0.776 ± 0.014	0.775 ± 0.010	0.785 ± 0.005	0.734 ± 0.005	0.734 ± 0.003
Model Misspecification	JS (Anisotropic)	—	0.837 ± 0.037	0.761 ± 0.040	0.791 ± 0.032	0.726 ± 0.015	0.736 ± 0.011
	JS (Laplace vs. Gaussian)	—	—	0.767 ± 0.015	0.861 ± 0.016	1.052 ± 0.017	1.227 ± 0.015
	KL (t -dist vs. Gaussian)	$df = 3$	—	0.164 ± 0.023	0.218 ± 0.017	0.267 ± 0.015	0.268 ± 0.010
	JS (GMM vs. Gaussian)	$\Delta = 1.0$	—	0.923 ± 0.006	0.759 ± 0.009	0.753 ± 0.007	1.012 ± 0.009

Table 3: Ratio summary across dimensions (d). Values report mean \pm standard deviation over 10 runs.

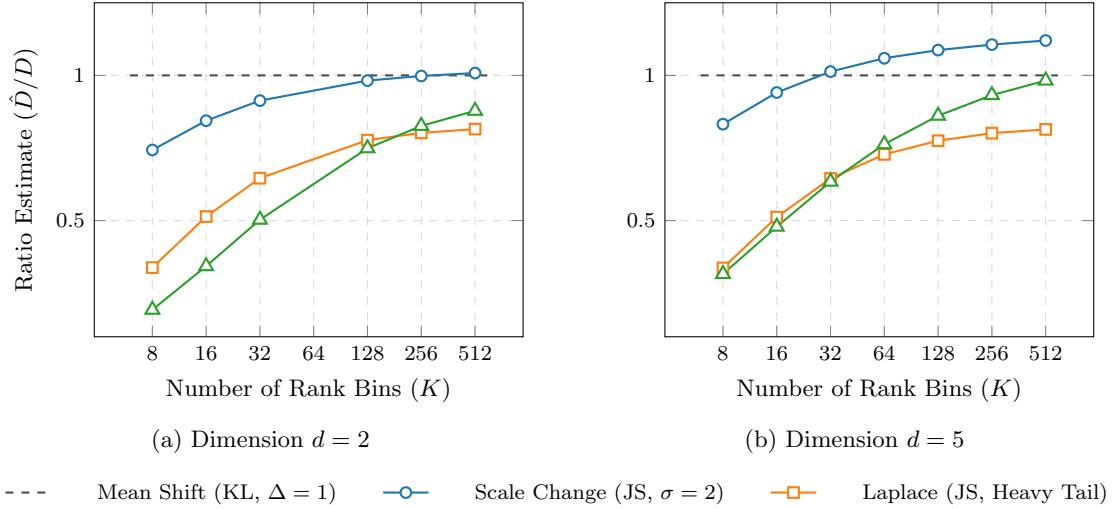


Figure 10: Convergence of ratio estimates (\hat{D}/D) versus number of rank bins (K) for dimensions $d = 2$ (left) and $d = 5$ (right).

C.4 Generative transport dynamics for rank-statistic f -divergences

We next provide pseudocode for the sliced rank–proximal transport update used in Section 4.4.

Algorithm 1 Sliced rank–proximal transport (one outer step)

Input: particles $(x_i)_{i=1}^N \subset \mathbb{R}^d$, reference samples $(y_j)_{j=1}^M \subset \mathbb{R}^d$, slices L , rank order K , temperature τ , trust η , step size ε , f -generator $f(\cdot)$.
Output: updated particles $(x_i)_{i=1}^N$.
Draw directions $s_1, \dots, s_L \in \mathbb{S}^{d-1}$ (optionally include antithetic pairs $\pm s_\ell$)
Initialize $\Delta x_i \leftarrow 0 \in \mathbb{R}^d$ for all $i = 1, \dots, N$
for $\ell = 1$ **to** L **do**
 Project: $x_i^{(\ell)} \leftarrow \langle x_i, s_\ell \rangle$, $y_j^{(\ell)} \leftarrow \langle y_j, s_\ell \rangle$
 Soft ranks: $U_{0,i}^{(\ell)} \leftarrow \hat{F}_{\nu^{(\ell)}}(x_i^{(\ell)}; \tau) \in (0, 1)$
 Prox in rank space (approx. by SGD/ULA/MALA):

$$U_1^{(\ell)} \approx \arg \min_{U \in (0,1)^N} \left\{ D_f(\hat{Q}^{(K)}(U) \| U_K) + \frac{1}{2\eta} \|U - U_0^{(\ell)}\|_2^2 \right\}$$

 (Optional) Monotone coupling: reorder $U_1^{(\ell)}$ to be nondecreasing in $x^{(\ell)}$
 Quantile match: $z_i^{(\ell)} \leftarrow (\hat{F}_{\nu^{(\ell)}})^{-1}(U_{1,i}^{(\ell)})$, $\delta_i^{(\ell)} \leftarrow z_i^{(\ell)} - x_i^{(\ell)}$
 (Optional) Clip $\delta_i^{(\ell)}$ for stability
 Accumulate: $\Delta x_i \leftarrow \Delta x_i + \delta_i^{(\ell)} s_\ell$
end for
Update: $x_i \leftarrow x_i + \varepsilon \frac{d}{L} \Delta x_i \quad$ for all i
return $(x_i)_{i=1}^N$

C.5 CelebA experiments

In this appendix we provide the experimental details underlying Section 4.4.2.

Center–outward rank–proximal transport (CO-RPT) Algorithm 2 implements a slice-free variant of rank–proximal transport based on a center–outward decomposition. Starting from particles $X = \{x_i\}_{i=1}^N$ and reference samples $Y = \{y_j\}_{j=1}^M$, we first recenter the configuration using the target mean $\bar{y} = \frac{1}{M} \sum_{j=1}^M y_j$, i.e., $\tilde{x}_i = x_i - \bar{y}$ and $\tilde{y}_j = y_j - \bar{y}$. Optionally, we apply a whitening transform (e.g. ZCA fitted on \tilde{Y}) so that the target is approximately isotropic; this reduces anisotropy and makes the radial/angular decomposition more stable, and the inverse transform is applied at the end.

We then decompose each point into its radius and direction: $r_i^x = \|\tilde{x}_i\|$, $u_i^x = \tilde{x}_i / r_i^x$ and $r_j^y = \|\tilde{y}_j\|$, $u_j^y = \tilde{y}_j / r_j^y$. The transport step is built by updating radii through a one-dimensional rank–proximal refinement, and updating directions through a simple matching on the unit sphere. Concretely, we compute soft radial ranks $U_{0,i} \approx \hat{F}_{r^y}(r_i^x) \in [0, 1]$ using a smoothed empirical CDF of the target radii, where the temperature τ controls how sharp the rank assignment is. We refine these ranks by

approximately solving the proximal objective

$$U_1 \approx \arg \min_{U \in (0,1)^N} \left\{ D_f(\widehat{Q}^{(K)}(U) \| U_K) + \frac{1}{2\eta} \|U - U_0\|_2^2 \right\},$$

where $\widehat{Q}^{(K)}(U)$ is the Bernstein-smoothed histogram over $[K]$ induced by U , $D_f(\cdot \| U_K)$ measures deviation from uniformity, and $\eta > 0$ acts as a trust region that prevents overly aggressive rank updates. In practice we use only a few inner iterations (e.g. SGD or a simple extragradient update). The refined ranks are mapped back to the radial axis via the empirical quantile of the target radii, $r_i^* = \widehat{F}_{r^y}^{-1}(U_{1,i})$, ensuring that uniform ranks would reproduce the target radial distribution.

To align angular structure, we match each particle direction u_i^x to a nearby target direction using cosine similarity, i.e. $j^*(i) \in \arg \max_j \langle u_i^x, u_j^y \rangle$, and blend toward it with weight $\beta \in [0, 1]$: $u_i^* = \text{normalize}((1 - \beta)u_i^x + \beta u_{j^*(i)}^y)$. Setting $\beta = 0$ yields a purely radial update, while larger β accelerates angular adaptation. Combining the transported radius and direction gives the center-outward proposal $\tilde{x}_i^* = r_i^* u_i^*$, and we take an outer step $\tilde{x}_i^+ = \tilde{x}_i + \varepsilon(\tilde{x}_i^* - \tilde{x}_i)$ with step size $\varepsilon > 0$. Optionally, we clip the increment to a maximum norm c to avoid rare large jumps. Finally, we undo the optional whitening and add back the center \bar{y} to obtain the updated particles $X^+ = \{x_i^+\}_{i=1}^N$.

Overall, CO-RPT replaces the multi-slice quantile matching of (9) by a single univariate rank-prox update on radii together with a lightweight spherical matching for directions. This yields a geometrically interpretable, fully sample-based update that explicitly controls the radial marginal through the rank objective, while encouraging directional alignment through nearest-neighbor coupling on \mathbb{S}^{d-1} .

Algorithm 2 Center-outward rank-proximal transport (CO-RPT) update

Input: particles $X = \{x_i\}_{i=1}^N$, targets $Y = \{y_j\}_{j=1}^M$, K, f, τ, η , step ε , angular blend β (optional cap c).
Output: updated particles X^+
 (Optional) center/whiten: \tilde{x}_i, \tilde{y}_j .
 Compute radii/directions: $r_i^x = \|\tilde{x}_i\|$, $u_i^x = \tilde{x}_i / r_i^x$ and $r_j^y = \|\tilde{y}_j\|$, $u_j^y = \tilde{y}_j / r_j^y$.
 Soft radial ranks: $U_0 \approx \widehat{F}_{r^y}(r^x) \in (0,1)^N$ (temperature τ).
 Prox in rank space: $U_1 \approx \arg \min_U \left\{ D_f(\widehat{Q}^{(K)}(U) \| U_K) + \frac{1}{2\eta} \|U - U_0\|_2^2 \right\}$.
 Target radii: $r^* \leftarrow \widehat{F}_{r^y}^{-1}(U_1)$.
 Angular match: $j^*(i) \in \arg \max_j \langle u_i^x, u_j^y \rangle$, $u_i^* \leftarrow \text{normalize}((1 - \beta)u_i^x + \beta u_{j^*(i)}^y)$.
 Proposal: $\tilde{x}_i^* \leftarrow r_i^* u_i^*$, $\Delta_i \leftarrow \tilde{x}_i^* - \tilde{x}_i$ (optional: $\Delta_i \leftarrow \Delta_i \cdot \min\{1, c/\|\Delta_i\|\}$).
 Update: $\tilde{x}_i^+ \leftarrow \tilde{x}_i + \varepsilon \Delta_i$ and uncenter/unwhiten to get x_i^+ .
return $X^+ = \{x_i^+\}_{i=1}^N$

Experimental setup and evaluation. We ran the proposed center-outward rank-proximal transport (CO-RPT) directly in pixel space on CelebA. We randomly selected $M = 1000$ images from the CelebA training folder, center-cropped and resized them to 64×64 , and mapped pixel intensities to $[0, 1]$; each image was then flattened to \mathbb{R}^{3HW} with $H = W = 64$. Unless stated otherwise, we used the Jensen-Shannon generator ($f = \text{JS}$) with trust-region parameter $\eta = 0.5$ and 3 inner extragradient steps per outer iteration. We initialized $N = M$ particles from a Gaussian

matched to the mean and marginal standard deviation of the whitened target features, and iterated CO-RPT for $T = 20000$ outer steps. We linearly annealed the rank resolution from $K = 96$ to $K = 224$, the rank-smoothing temperature from $\tau = 0.30$ to 0.07 , and the outer step size from $\varepsilon = 0.16$ to 0.10 , while clipping per-particle updates to a maximum norm of $c = 0.30$.

C.6 Addressing mode collapse on MNIST

Building on the pretraining approach of [12], who employ a rank-based total-variation divergence to reduce mode collapse in GANs, we study whether the same strategy carries over to a wider class of rank-statistic f -divergences. Concretely, we incorporate the sliced rank-statistic f -divergences objective as a pretraining signal for the DCGAN generator [43] and evaluate the resulting pipeline on MNIST. To measure both realism and coverage, we follow [47] and report precision (as a proxy for fidelity) and recall (as a proxy for diversity). All models are trained for 40 epochs with batch size 128. For the pretrained variants, we first run 20 epochs under the sliced rank-statistic f -divergences objective and then continue with 40 additional epochs of standard DCGAN training.

In Table 4, we compare *rank-statistic f -divergence* pretraining variants (TV, KL, JS, and Hell²) with standard DCGAN training, *rank-statistic f -divergence*+DCGAN fine-tuning, and stronger multi-discriminator baselines [9, 16]. Focusing on precision and recall, the standalone *rank-statistic f -divergence* models already achieve strong recall on MNIST: JS and Hell² are the most recall-oriented, reaching 97.0% and 98.7% recall for $m=50$, respectively, while TV and KL yield a more balanced behaviour (e.g., 95.0% and 91.1% recall for $m=50$). When we pretrain with a *rank-statistic f -divergence* and then fine-tune with the adversarial loss, precision increases substantially relative to vanilla DCGAN: TV+DCGAN and KL+DCGAN reach 95.0% and 96.2% precision, respectively (vs. 93.85% for DCGAN), while maintaining competitive recall (around 92.8% and 90.5%). Overall, these results highlight a clear trade-off between the choice of f (more recall-oriented for JS/Hell²) and the benefit of adversarial fine-tuning for improving precision without collapsing recall.

D Limitations and future work

The proposed rank-statistic construction reduces divergence estimation to operations on ranks and histograms, yielding a fully sample-based surrogate that avoids explicit density-ratio modelling. At the same time, several limitations remain, many of which are shared by other projection-averaging objectives. In particular, the multivariate variant is defined by averaging a univariate discrepancy over random one-dimensional projections. While projection families can characterize distributions in the limit, any finite number of directions L can miss informative orientations, especially when the discrepancy is concentrated in a low-dimensional subspace, encoded in rare but important directions, or dominated by higher-order dependence patterns. Similar phenomena are documented for sliced objectives in optimal transport and generative modelling [24]. A practical implication is that performance can depend non-trivially on L and on how directions are sampled, and diagnosing “missed directions” may be difficult without problem-specific insight.

A second limitation is that the surrogate is inherently discretized through the resolution parameter K . Although the theoretical analysis establishes monotonicity and consistency as $K \rightarrow \infty$, the choice of a finite parameter K induces approximation error and may distort the geometry of the objective. This is particularly relevant when the divergence is used as a learning signal: the discretization can alter local sensitivity and may emphasize coarse distributional differences over fine structure. Developing principled, data-dependent rules for selecting K (and, in the sliced case, jointly selecting

Dataset	Method	F-score		P&R	
		$F_{1/8} \uparrow$	$F_8 \uparrow$	Precision \uparrow	Recall \uparrow
MNIST	TV (m=20)	88.09 ± 0.32	93.91 ± 0.72	88.01 ± 0.52	94.25 ± 0.91
	TV (m=50)	88.89 ± 0.31	94.90 ± 0.71	88.80 ± 0.50	95.08 ± 0.94
	KL (m=20)	90.50 ± 0.43	90.21 ± 0.62	90.50 ± 0.47	90.18 ± 0.91
	KL (m=50)	91.59 ± 0.46	91.11 ± 0.68	91.62 ± 0.47	91.11 ± 0.88
	JS (m=20)	86.64 ± 0.56	96.13 ± 0.76	86.48 ± 0.40	96.32 ± 0.92
	JS (m=50)	87.73 ± 0.32	96.84 ± 0.75	87.60 ± 0.49	97.09 ± 0.91
	Hell ² (m=20)	83.00 ± 0.35	97.92 ± 0.74	82.81 ± 0.50	98.23 ± 0.87
	Hell ² (m=50)	83.83 ± 0.35	98.43 ± 0.69	83.62 ± 0.50	98.71 ± 0.90
	DCGAN	93.54 ± 0.64	75.66 ± 1.46	93.85 ± 1.45	75.43 ± 2.56
	TV + DCGAN	94.97 ± 0.35	92.83 ± 0.72	95.00 ± 0.53	92.80 ± 0.85
	KL + DCGAN	96.11 ± 0.36	90.58 ± 0.70	96.20 ± 0.46	90.50 ± 0.83
	JS + DCGAN	94.71 ± 0.42	95.19 ± 0.73	94.67 ± 0.42	95.21 ± 0.87
	Hell ² + DCGAN	93.84 ± 0.35	96.75 ± 0.75	93.82 ± 0.45	96.81 ± 0.85
	GMAN	97.78 ± 0.40	96.52 ± 0.57	97.80 ± 0.71	96.53 ± 0.89
	MCL-GAN	98.20 ± 0.19	98.00 ± 0.25	98.20 ± 0.30	98.00 ± 0.40

Table 4: Quantitative results on MNIST (28×28), reporting $F_{1/8}$ and F_8 (the β -weighted harmonic means of precision and recall), precision, and recall (mean \pm std, %). Results are grouped by divergence type for enhanced scannability.

(K, L)) remains an open problem. Promising directions include selection via held-out calibration, adaptive schedules that increase K over training, and criteria based on stability of estimates across nearby resolutions.

Third, the sliced rank-statistic construction inherits an accuracy-compute trade-off from Monte Carlo integration on the sphere. In high dimensions, each projection reduces the problem to a 1D rank histogram, but capturing direction-dependent mismatch may require many directions L . Increasing L improves coverage of informative orientations and typically reduces Monte Carlo variability through averaging, yet the overall cost grows roughly linearly in L (and also increases with the rank resolution K through the histogram/Bernstein evaluation). At realistic scales, this can make the sliced surrogate expensive, whereas using too few directions risks missing informative projections and yielding overly optimistic (or misleading) discrepancy estimates—a limitation shared by other sliced objectives [24].

Several extensions could increase the information per projection beyond i.i.d. random directions. One option is to replace purely random directions with structured ensembles that reduce redundancy (e.g., near-orthogonal directions) or with low-discrepancy point sets on the sphere, which can lower projection variance at fixed L compared to standard Monte Carlo [15, 50]. Another direction is data-dependent slicing: rather than sampling s uniformly, directions can be biased toward projections where the (rank-based) discrepancy is largest, connecting to max-sliced and projection-pursuit ideas [14, 41]. More generally, one could adapt learned slicing to the rank-statistic setting by choosing

projection directions in a learned feature space, or by learning a small set of directions jointly with the generator so that each slice is maximally informative [25]. Recent analyses of sliced distances and direction sampling also suggest that careful design of projection sets can provide better statistical efficiency and stronger practical guarantees [39].

Fourth, it would be valuable to place the sliced rank–statistic f –divergence in a more formal “flow” framework, in the same spirit as sliced–Wasserstein flows [32]. Concretely, one can view the sliced rank objective as defining a functional on probability measures whose descent induces transport dynamics: at each time step, projected one–dimensional rank corrections define a drift field that moves particles toward the data distribution, while optional entropy/noise terms control dispersion and prevent collapse. A theory along these lines could clarify the accuracy–compute trade–off introduced by slicing (finite L directions) and discretization (finite K), and could enable finite–time guarantees for particle discretizations that explicitly track how the error depends on (m, K) and step sizes, mirroring the role of Monte Carlo slicing and time discretization in flow–based analyses [32].

In parallel, these transport dynamics suggest an amortized alternative: instead of running particle updates at test time, a generator could be trained to emulate one (or a few) steps of rank–proximal transport, or to directly map base noise to samples that minimize the sliced rank divergence. Such amortization could dramatically reduce the per–iteration cost at image scale.

Finally, empirical evaluation can be broadened along several axes. The current experiments emphasize synthetic settings and representative implicit learning tasks, but more diverse benchmarks (including larger–scale image generation, text/sequence data, and domain adaptation scenarios, and time-series forecasting) would better delineate when rank–statistic divergences outperform classical and neural alternatives. In addition, ablations that isolate the effects of K , L , projection sampling, and batching would help translate theoretical guarantees into robust practitioner guidance. Extensions to conditional divergences, two–sample testing, and settings with nuisance variables (e.g., covariate shift) are also natural, since rank constructions are compatible with sample–based pipelines and may be combined with representation learning.

E Experimental Setup

All experiments were performed on a MacBook Pro running macOS 13.2.1, equipped with an Apple M1 Pro CPU and 16 GB of RAM. When GPU acceleration was required, we used a single NVIDIA TITAN Xp with 12 GB of VRAM. Detailed hyperparameter settings for each experiment are provided in the corresponding sections. An anonymous repository containing all code and data is available at <https://anonymous.4open.science/r/rsfdiv-2C8A/>.